P874

FERMILAB-Proposal-0874 **27th March 1995**

P874: A Proposal to Measure the π^+ and π^- Lifetimes at High Energy

J. Freeman, S. Geer[†], C. Hojvat[#], C. Johnstone, J. Streets, D. Striley[*]

Fermi National Accelerator Laboratory, P.O. Box 500, Batavia, IL 60510

L. DeMortier, N.D. Giokaris, D.M. Khazins

Experimental Physics Dept., Rockefeller University, New York, NY 10021-6399

S. Oh, T.J. Phillips, C. Wang

Physics Dept., Duke University, Durham, NC 27706

G. Snow, C. Lundstedt

Dept. of Physics and Astronomy, 116 Brace Hall, University of Nebraska, Lincoln, NE 68588-0111

Abstract

We propose to make precise measurements of the π^+ and π^- lifetimes at high energy. A comparison of the $\pi^\pm$ lifetimes at the highest Fermilab energies with the measured lifetimes at rest would test the time dilation formula for particle decays at the highest energies and Lorentz boosts available in the laboratory. In addition, a comparison of the π^+ lifetime with the π^- lifetime at high energy would provide us with a test of the CPT theorem in a unique region of parameter space. Within the framework of some specific models we expect our proposed measurements to be sensitive to a Lorentz non-invariant or CPT violating interaction at a distance scale of order 10^{-18} cm, or a Lorentz non-invariant or CPT violating component of the normal weak interaction Hamiltonian at the level of one part in 10^{10}.

(†) Spokesperson, (#) Co-Spokesperson, (*) Visitor

AAU 8317

1 Introduction

The Fermilab Tevatron produces the highest energy meson beams in the world, and therefore offers a unique opportunity to test the time dilation formula ($\tau = \gamma\tau_0$) for weakly decaying particles at the highest energies and Lorentz boosts available in the laboratory. A deviation from the time dilation formula at high energy would indicate the presence of a Lorentz non-invariant interaction at small distance scales. In addition, a difference between particle and antiparticle lifetimes at high energy would indicate the presence of a CPT violating interaction. Although we have no deep theoretical reason to suspect a violation of Lorentz invariance or a violation of the CPT theorem, these are two of the most fundamental principles of modern physics and it is therefore of interest to test them in as many ways as possible.

During the coming Fermilab fixed target run we propose to make precise measurements of the π^+ and π^- lifetimes at the highest energies that are practical at Fermilab. In particular, we propose to measure the π^+ and π^- lifetimes at 530 GeV ($\gamma = 3797$) with precisions of 0.1%. We plan to determine the lifetimes by measuring the fraction of pions that decay whilst traversing 100m, 50m, and 30m long decay lengths. Precise momentum measurements at the upstream and downstream ends of the decay region together with good muon identification will enable pion decays to be cleanly identified. In addition to our proposed pion lifetime measurements we note that we may also be able to make precise measurements of the K^+ and K^- lifetimes at high energy. This is presently under study.

Our measurements would provide us with a search for a Lorentz non-invariant interaction or a CPT violating interaction at very small distance scales. In particular, within the framework of some specific models discussed in the following sections, we expect our measurements to be sensitive to a Lorentz non-invariant or CPT violating interaction at distance scales as small as a few times 10^{-18} cm, or a Lorentz non-invariant or CPT violating component of the normal weak interaction Hamiltonian at the level of one part in 10^{10}.

Table 1 summarizes results from existing high energy lifetime measurements for weakly decaying particles. The precisions of the highest energy measurements are all of order 1%. The highest energy lifetime measurement is for the K_S^0 at 375 GeV ($\gamma = 754$) for which the

lifetime has been determined with a precision of 6.8%. Thus our proposed high energy π^+ and π^- lifetime measurements would (i) test the time dilation formula with a precision that is about an order of magnitude better than the precisions achieved by existing high energy lifetime measurements, and (ii) test Lorentz invariance in weak decays at Lorentz boosts that are a factor of 5 higher than the K_S^0 measurement. Within the framework of some explicit models of Lorentz non-invariance which are discussed in the following sections, the sensitivity of high energy particle lifetimes to new Lorentz non-invariant physics is expected to be proportional to the square of the energy or γ^2 of the decaying particle. Hence, within the framework of these models, compared to existing high energy lifetime measurements our proposed π^+ and π^- measurements would be more sensitive to a Lorentz non-invariant interaction by more than an order of magnitude.

Table 2 summarizes existing precision measurements of the $\pi^\pm$ lifetime reported in the literature. The lifetime at rest has been determined with a precision of 0.1%. Only a few measurements of the $\pi^\pm$ lifetimes have been made for pions in flight. The only measurements reported in the literature for $\pi^\pm$ with momenta greater than 1 GeV/c are those of Lobkowicz et al. [1] who measured pion lifetimes at 1.8 ± 0.2 GeV/c ($\gamma = 13$). Thus our proposed measurements of the π^+ and π^- lifetimes at 530 GeV would test the time dilation formula for these decays at Lorentz boosts that are more than two orders of magnitude larger than any previous precision $\pi^\pm$ measurements.

2 Sensitivity to New Physics at Small Distance Scales

The success of the standard model in describing the worlds electroweak data implies that if there is a Lorentz non-invariant or CPT violating interaction it probably occurs at a distance scale much smaller than the weak scale which is $O(10^{-16})$ cm. Indeed, the ability of the standard model to describe even the hardest collisions recorded by CDF and D0 at the Fermilab Tevatron collider suggests that any Lorentz non-invariant or CPT violating interaction that exists probably occurs at distance scales smaller than a few times 10^{-17} cm. We can therefore assume that if there is an observable breakdown of Lorentz invariance or a violation of the CPT theorem it will manifest itself as a small correction to standard model predictions associated with physics at a distance scale of order 10^{-17} cm or less.

2.1 The Redei Model

A deviation from the time dilation formula $\tau = \gamma\tau_0$ at high energy would indicate the presence of new Lorentz non-invariant physics at small distance scales. Within the framework of a specific model describing the Lorentz non-invariant interaction the size of the lifetime deviation can be related to the distance scale on which the new Lorentz non-invariant interaction is taking place. One such specific model has been proposed by Blokhintsev [2] and developed by Redei [3] and by Lundberg and Redei [4]. In the Redei model microcausality is broken below some small fundamental distance scale α. The resulting weak interaction Hamiltonian contains a non-causal form factor that permits interaction between simultaneous space-time events in the laboratory frame provided their spatial separation is less than α. The time dilation formula for the decay of a particle of mass m is then modified:

$$\tau = \gamma\tau_0 \{1 + 0.2(mc/\hbar)^2\gamma^2\alpha^2\} = \gamma\tau_0 \left\{1 + 0.2(E/\hbar c)^2\alpha^2\right\}. \tag{1}$$

Thus the lifetime at high energy would be longer than normally expected by an amount:

$$\Delta \equiv \tau/(\gamma\tau_0) - 1 = 0.2(E/\hbar c)^2\alpha^2. \tag{2}$$

Expressing α in cm and energy E in GeV, this yields:

$$\Delta = 5 \times 10^{26}\, E^2\alpha^2. \tag{3}$$

We can now ask "what is the minimum beam energy required to probe the range $\alpha \leq 10^{-17}$ cm if the lifetime is measured with good precision ?". Figure 1 shows as a function of the energy of the decaying particle the value of α that will result in a deviation Δ of 0.1%. Particle decays at energies in excess of 100 GeV begin to probe the interesting region. For a given α the magnitude of the expected deviation Δ increases as the square of the beam energy. Hence it is important to make measurements at the highest practical beam energies. We propose to measure the π^+ and π^- lifetimes up to energies of 530 GeV. In Fig. 2 the expected deviation from the time dilation formula is shown as a function of α for particles with an energy of 530 GeV. We conclude that at 530 GeV we need to measure the $\pi^\pm$ lifetimes with a precision of 1% or better to probe the region $\alpha \leq 10^{-17}$ cm. Finally, we note that if the high energy lifetime is measured with the same level of precision achieved in

the measurement of the $\pi^{\pm}$ lifetime at rest (0.1%) then a two standard deviation difference between τ and $\gamma\tau_0$ corresponds to $\Delta = 0.0027$. At 530 GeV this corresponds to a value for α of:

$$\alpha = \ (8.3 \times 10^{-17})\, \Delta^{1/2}\ cm = \ 4 \times 10^{-18}\ cm. \tag{4}$$

Thus, our proposed high energy π^+ and π^- lifetime measurements would test Lorentz invariance and the CPT theorem at distance scales less than a few times 10^{-17} cm. Indeed, within the framework of the Redei model our proposed measurements probe distance scales that are a factor of 60 smaller than the typical weak interaction scale ($\hbar c/m_W = 2.5 \times 10^{-16}$ cm), and an order of magnitude smaller than the scale probed directly by the hardest parton-parton collisions observed by CDF and D0.

2.2 Existing Limits

Searches for a Lorentz non-invariant interaction can be made by measuring any Lorentz invariant quantity as a function of γ. Examples are τ/γ, particle masses, and cross-sections at a given center-of-mass energy. The energy dependent lifetimes of weakly decaying particles offer a particularly attractive way to search for deviations from Lorentz invariance since many of these lifetimes have been measured at rest with good precision and it is possible to make precise measurements of particle lifetimes at the highest available energies and hence largest Lorentz boosts.

A compilation of particle lifetime measurements for weakly decaying particles at the lowest and highest energies reported in the literature is given in Table 3. These measurements are all consistent with the time dilation formula with the possible exception of the $\pi^{\pm}$ results which give a value for Δ which is 2.7σ from zero. The agreement between the time dilation formula and the measured lifetimes at low and high energies can be used to place upper limits on the fundamental Redei length α. The resulting limits on α are listed in Table 4. The most stringent limit is obtained from a comparison of the K_S^0 lifetime at 375 GeV [5] with the lifetime at 2 GeV, which yields $\alpha \leq 4.4 \times 10^{-17}$ cm (at 2σ). This distance scale is competitive with the scales probed by the hardest collisions recorded at the Tevatron proton-antiproton collider, but is an order of magnitude larger than the smallest distance scale that would be probed by our proposed pion lifetime measurements.

Newman et al [6] have suggested that an alternative way of searching for a Redei-like modification of Special Relativity is to look for an energy dependence in the measured electron and muon values of g-2. They introduce a parameter C_1 which quantifies as a function of energy the difference between the effective Lorentz boost $\overline{\gamma}$ and the expected boost γ. The parameter C_1 is related to the parameter Δ discussed above :

$$C_1 \;= \frac{1}{\overline{\gamma}} - \frac{1}{\gamma} \;= -\,\overline{\gamma}\,\Delta. \tag{5}$$

The most stringent limit on C_1 comes from the measured g-2 of the electron at 12 GeV which gives $C_1 < 1.6 \times 10^{-9}$ (at 2σ) [7]. This corresponds to an upper limit on the Redei length α of 1.0×10^{-16} cm, which is not competitive with limits from particle lifetime measurements at high energies.

3 Lorentz Non-Invariance in Weak Interactions

Our proposed π^+ and π^- lifetime measurements will enable us to search for evidence of a Lorentz non-invariant or CPT-violating contribution to weak decays. It is therefore interesting to understand the sensitivity of our proposed measurements within the framework of a model in which the standard theory of electroweak interactions has been modified by the addition of a Lorentz non-invariant interaction. A model of this type has been proposed by Nielsen and Picek [8]. Unfortunately the Nielsen and Picek model implies a modification of the Dirac equation for electrons which is thought to be unacceptably large. Never-the-less the Nielsen and Picek model has some general features which make it useful in providing a framework within which we can compare the sensitivities of various experimental searches to the presence of a Lorentz non-invariant interaction. In particular the model is simple, highly predictive, and illustrates the way in which a new Lorentz non-invariant interaction can manifest itself as an energy dependent correction to the normal time dilation formula.

3.1 The Nielsen and Picek Model

In their model, Nielsen and Picek change the W and Z^0 boson propagators of the standard model:

$$D_{\mu\nu}(x-y) \;=\; (-ig_{\mu\nu}/m^2_{W,Z})\delta^4(x-y) \tag{6}$$

by introducing a small Lorentz non-invariant addition $\chi_{\mu\nu}$ to the normal metric tensor $g_{\mu\nu}$:

$$g_{\mu\nu} \;\rightarrow\; g_{\mu\nu} + \chi_{\mu\nu}. \tag{7}$$

The Lorentz non-invariant term arises from additional non-scalar couplings in the Higgs sector, and is therefore associated with the generation of heavy gauge boson masses. This modification to the standard model results in an effective current-current interaction:

$$H_{eff} \;=\; (G/\sqrt{2})(g_{\mu\nu} + \chi_{\mu\nu})\left\{J^{\mu\dagger}(x)J^{\nu}(x)\right\}. \tag{8}$$

After requiring rotational invariance the Lorentz non-invariant tensor $\chi_{\mu\nu}$ is found to have the form $\chi_{00} = \delta$, $\chi_{11} = \chi_{22} = \chi_{33} = \delta/3$. Thus there is a single fundamental parameter δ which characterizes the size of the Lorentz non-invariant addition to $g_{\mu\nu}$. To understand the nature of the Lorentz non-invariant effects that are introduced by this model consider the quantity $g_{\mu\nu}p^\mu p^\nu$. In the standard model:

$$-\,g_{\mu\nu}p^\mu p^\nu \;=\; m^2. \tag{9}$$

In the model of Nielsen and Picek:

$$-\,g_{\mu\nu}p^\mu p^\nu \;=\; m^2 \;-\; \delta(\frac{1}{3}p^2 + p_0^2) \tag{10}$$

which is clearly not Lorentz invariant. The mass m depends on the velocity of the frame of reference with respect to some preferred frame. This is similar to the behavior that arises when Lorentz non-invariant effects are due to an external field whose sources are at rest in the preferred frame.

The Lorentz non-invariant addition to the weak interaction Hamiltonian results in a modification to the usual time dilation formula describing the energy dependence of particle lifetimes. Nielsen and Picek have explicitly calculated this modification for the weak decays of

leptons and mesons. They find that the symmetry properties of the Lorentz invariant and non-invariant terms result in selection rules which suppress the sensitivities of some decay modes to the presence of $\chi_{\mu\nu}$. In particular, the sensitivities of the energy dependent $\mu^{\pm}$, $\tau^{\pm}$, K_S^0, and K_L^0 lifetimes to the Lorentz non-invariant interaction are suppressed, whilst the sensitivities of the $\pi^{\pm}$ and $K^{\pm}$ lifetimes are not suppressed. Nielsen and Picek therefore stress the importance of making precise high energy measurements of the $\pi^{\pm}$ and $K^{\pm}$ lifetimes.

In the Nielsen and Picek model the time dilation formula for $\pi^{\pm}$ decay is modified:

$$\tau = \gamma\tau_0 \{1 + (4/3)\delta\gamma^2\}^{-1} \sim \gamma\tau_0 \left\{1 - (4/3)\delta\gamma^2\right\}. \tag{11}$$

Thus the pion lifetime at high energy would be different than expected by an amount:

$$\Delta \equiv \tau/(\gamma\tau_0) - 1 = -(4/3)\delta\gamma^2. \tag{12}$$

The predicted deviation Δ is shown in Fig. 3 as a function of the fundamental parameter δ for $\pi^{\pm}$ decaying at 530 GeV. A measurement of the $\pi^{\pm}$ lifetime with a precision of 0.1% would yield a difference between τ and $\gamma\tau_0$ greater than two standard deviations ($\Delta = 0.0027$) if the fundamental parameter $\delta > 1.4 \times 10^{-10}$. This is a factor of 6×10^5 more sensitive than limits on δ from the existing $\pi^{\pm}$ lifetime measurements listed in Table 3.

3.2 Existing Limits

Several methods have been proposed for searching for a Lorentz non-invariant interaction of the type proposed by Nielsen and Picek. The relationships between δ and the following have been explicitly discussed in the literature:

- The energy dependent $\pi^{\pm}$, $K^{\pm}$, and hyperon lifetimes.
- The muon Michel parameter.
- The energy dependent $K_L - K_S$ mass difference.
- Modifications of the weak interaction contributions to the nuclear binding energy that would affect the gravitational acceleration of a test mass and lead to positive results in Eötvos experiments.

Results from these measurements are summarized in Table 5 and are discussed in more detail in Appendix 1. Note that the values of δ extracted from the hyperon lifetime measurements are based on the calculations of Huerta and Lucio [9] who obtain a similar expression to the one given by Nielsen and Picek for pion decay, except that the factor of (-4/3) is replaced by an unknown factor c_2. The results in Table 5 are obtained by assuming $c_2 = 1$, which Huerta and Lucio argue is reasonable. All the existing results listed in Table 5 are consistent with $\delta = 0$. The most stringent limits on δ come from measurements of the energy dependent $K_L - K_S$ mass difference and the energy dependent Ξ^- lifetime. The resulting upper limit on the fundamental parameter δ is 8.7×10^{-6}. Thus, within the framework of the Nielsen and Picek model, our proposed high energy pion lifetime measurements are expected to be sensitive to non-zero values of the fundamental parameter δ that are almost five orders of magnitude smaller than the values currently excluded by the measurements listed in the table.

4 Experimental Considerations

We next consider the general characteristics of an experiment designed to measure the π^+ and π^- lifetimes at high energy. To be definite, we consider an experiment which determines the $\pi^\pm$ lifetime by measuring the decays of 530 GeV pions as they traverse an experimental decay region. The $\pi^\pm$ decay length at 530 GeV is 29.6 Km. The existing facilities at Fermilab can accommodate a decay region of about 100 m length. Hence, in practice, the experimental decay region will be small compared to the decay length, and the decay vertices will be distributed nearly uniformly along the length of the decay region. The pion lifetime can be determined by measuring the fraction $f(L)$ of pions that decay whilst traversing a decay region of length L:

$$f(L) \;=\; 1 \;-\; e^{-L/\gamma c\tau}. \tag{13}$$

With $L = 100$m and $\gamma = 3797$ we expect $f = 0.0034$. A precise measurement of τ requires precise measurements of f, L, and γ.

Consider $\pi^\pm \rightarrow \mu^\pm\nu$ decays. The predicted distributions of muon energies and angles are shown in Figs. 4 and 5 for the decays of 530 GeV pions. The muon energies are uniformly

distributed between a minimum energy of 300 GeV and a maximum energy of 530 GeV. The muon directions are practically collinear with the initial $\pi^{\pm}$ direction, the maximum decay angle being less than 80 microradians. Thus a $\pi^{\pm} \rightarrow \mu^{\pm}\nu$ decay candidate can be identified with a beam particle which has the selected momentum and direction at the upstream end of the decay region, and results in a single lower momentum particle identified as a muon at the downstream end of the decay region. This facilitates the measurement of f. However, in practice there are significant end effects associated with decays that take place within the magnetic field volumes of the upstream momentum selector or the downstream momentum analyzer. If the field maps and the experimental geometry are well known then in principle the end effects can be taken properly into account. However it is better to reduce these end effects by making two measurements with different decay lengths L_1 and L_2. The ratio of these measurements

$$R \equiv \frac{1-f_1}{1-f_2} = e^{-(L_1-L_2)/\gamma c\tau} \tag{14}$$

depends on the difference in the two decay lengths, which can be precisely determined, and does not have a contribution from end effects. The lifetime is then given by:

$$\tau = \frac{1}{\gamma c}\frac{(L_2 - L_1)}{\ln R}. \tag{15}$$

The uncertainty on the measured lifetime is given by:

$$\left(\frac{\sigma_\tau}{\tau}\right)^2 = \left(\frac{\sigma_\gamma}{\gamma}\right)^2 + \left(\frac{\sigma_{\ln R}}{\ln R}\right)^2 = \left(\frac{\sigma_p}{p}\right)^2 + \left(\frac{\sigma_R}{R\ln R}\right)^2 \tag{16}$$

where p is the beam momentum and we have neglected the uncertainty on $\Delta L = L_1 - L_2$ since in practice ΔL can be determined with high precision (better than 1 part in 10^5). If the fractions f_1 and f_2 are determined by recording respectively N_1 and N_2 decays, then it can be shown that:

$$\left(\frac{\sigma_\tau}{\tau}\right)^2 = \left(\frac{\sigma_p}{p}\right)^2 + \frac{a^2}{N_1} + \frac{b^2}{N_2} \tag{17}$$

where

$$a = \frac{f_1}{r(1-f_1)}, \quad b = \frac{f_2}{r(1-f_2)}, \text{ and } \quad r \equiv \ln\left(\frac{1-f_1}{1-f_2}\right). \tag{18}$$

For fixed lengths L_1 and L_2 the expected fractions f_1 and f_2 are known, and hence a and b can be computed. In general, for a given statistical precision we want to minimize the

required data taking time and hence choose $N_2 < N_1$ (where $L_2 < L_1$). The optimum choice that will yield a statistical precision on the lifetime:

$$\frac{\sigma_\tau}{\tau} = \frac{1}{\sqrt{N}} \tag{19}$$

is given by:

$$N_1 = N \times \left(a^2 + \sqrt{a^2 b^2 L_1/L_2}\right) \tag{20}$$

and

$$N_2 = N \times \frac{b^2 N_1}{N_1 - a^2 N} \,. \tag{21}$$

Taking $L_1 = 100$m, Table 6 shows as a function of the length L_2 the optimum choices for N_1 and N_2 required to achieve a statistical precision of 0.1%. As an example, if $L_1 = 100$m and $L_2 = 30$m then we need to record $N_1 = 3.2 \times 10^6$ decays and $N_2 = 5.0 \times 10^5$ decays. We are presently proposing to measure the decay fractions at three lengths (100m, 50m, and 30m). The addition of measurements at a third length provides a cross check of our results.

In addition to the statistical uncertainties on the measured lifetimes there are also a number of systematic uncertainties. We consider first the uncertainties that arise due to the presence of background events that result in fake pion decays. It is useful to consider the approximation:

$$R \equiv \tfrac{1-f_1}{1-f_2} \simeq 1 - f_1 + f_2 \,, \tag{22}$$

where we have neglected terms of order f^2. R can be written in terms of the observed decay fractions f^o and the background fractions b:

$$R \equiv \simeq 1 - (f_1^o - b_1) + (f_2^o - b_2) \,. \tag{23}$$

If the probability for an incoming beam particle to fake a pion decay is independent of the decay region length then the background fractions cancel and we obtain:

$$R \equiv \simeq 1 - f_1^o + f_2^o \,. \tag{24}$$

However, to allow for some variation in b with decay region length, and take account of the approximation of neglecting terms of order f^2, we will allow b_1 to be different from b_2 by 10%. In this case:

$$R \equiv \simeq 1 - f_1^o + f_2^o \pm (0.1 \times b) \,. \tag{25}$$

Hence, to ensure that our measured lifetime is accurate to 0.1% we must ensure that b is less than $1\% \times (f_1 - f_2) \simeq 10^{-5}$. With this in mind consider:

(i) Beam muons that fake decay muons. In practice, of order 1% of the beam particles incident at the upstream end of the decay region will be muons. The only discrimination between these beam muons and muons from pion decay comes from a comparison of the particle momenta at the upstream and downstream ends of the experiment. Therefore, to suppress beam muons faking decay muons we will need a precise momentum measurement at both ends of the decay region. We can then obtain a rejection factor of 10^3 by requiring that decay candidates have a momentum measured downstream of the decay region that is significantly lower than the momentum measured upstream of the decay region. The exact momentum difference requirement can be specified once the resolution functions of the momentum spectrometers have been determined. These resolution functions can be measured with a short 530 GeV/c run with protons or muons.

(ii) Non-decaying pions that fake decay muons. We need to ensure that the probability for beam pions to fake a decay muon is less than 10^{-5}. We will therefore need, in addition to the rejection that comes from our precise momentum measurements, a further factor of 100 in the discrimination between beam pions and decay muons.

We now consider the uncertainty on the lifetime that arises from our imperfect knowledge of the muon tagging efficiency. If $\epsilon_\mu > 0.999$ then the resulting correction to f will be 10^{-3} or less, the correction to R will be of order 10^{-6} or less, and the correction to the measured pion lifetime will be 0.1% or less. Therefore we will want the muon tagging efficiency to be close to unity, and the uncertainty on the muon tagging efficiency to be less than 0.1%.

Finally we consider the uncertainty on our lifetime determination that arises from the uncertainty on the incident number of beam pions. To ensure that we measure R correctly to within the required precision we must know the number of incident pions N_π with a precision of 0.1%. In our experiment we propose to use a differential Cherenkov counter to reject kaons and protons in the beam. We will therefore require that the mistag fraction associated with kaons or protons being misidentified as pions in the Cherenkov should be

less that 0.1%. In addition to this we expect of order 1% of the beam particles to be muons, which cannot be distinguished from pions in the Cherenkov counter. We must therefore determine the fraction of beam particles that are muons with a precision of better than 10%. This can be accomplished with the same muon tagging system that is needed to identify decay muons, provided this tagging system can discriminate between muons and pions with a pion rejection of at least 10^3.

We conclude that if we wish to measure the π^+ and π^- lifetimes at high energy with a precision of 0.1% then we must:

- Select beam particles of a given momentum and direction and determine γ and hence the central beam momentum to better than 0.1%,
- Measure the decay fractions at two different decay lengths L_1 and L_2, and measure the difference $(L_1 - L_2)$ with a precision of much better than 0.1%,
- Measure the decay fractions f_1 and f_2 by recording at least a few $\times 10^6$ decays at the longer decay length and a few $\times 10^5$ decays at the shorter decay length.
- Reduce the proton and kaon contaminations in the beam to much less than 0.1%.
- Measure the muon contamination in the beam with a precision of better than 10% which will require a rejection against beam pions faking a muon of greater than 10^3.
- Identify high energy muons with an efficiency known to better than 0.1%,
- Identify decay muons with a rejection against beam pions faking a decay muon of greater than 10^5 and a rejection against beam muons faking decay muons of better than 10^3. This will require a precise momentum determination at the upstream and downstream ends of the decay region to obtain a factor of 1000 rejection against beam muons faking decay muons, and a muon tagging system to obtain a further rejection of 100 against pions faking decay muons.

5 The Proposed Experiment

We propose to carry out our pion decay experiment in the Meson West (MW) beam line and experimental hall (MW9). The MW beam line fluxes have been measured up to momenta as high as 530 GeV/c, both for positive and negative secondaries. We propose to measure the π^+ and π^- lifetimes at 530 GeV and at one additional lower energy, which we provisionally take to be 100 GeV. The proposed apparatus is shown in Fig. 6. It consists of the following elements:

1. The existing MW differential Cherenkov counter (C).
2. An upstream magnetic spectrometer to enable the selection of beam particles with momenta within about 2% of the central beam momentum. The upstream spectrometer consists of two EPB magnets (EPB-1 and EPB-2), two sets of tracking chambers (T1 and T2), four trigger scintillators (S1, S2, S3, and S4), and a system of veto scintillators (V1, V2, V3, and V4).
3. A variable length decay pipe, shown 100m long (D), evacuated to minimize nuclear interactions.
4. A downstream magnetic spectrometer for measuring particle momenta downstream of the decay pipe. The downstream spectrometer consists of two EPB magnets (EPB-3 and EPB-4), two sets of tracking chambers (T3 and T4), the trigger scintillators (S5 and S6), and the veto scintillators (V5 and V6).
5. An electromagnetic calorimeter (ECAL) to identify electrons in the beam and reject accompanying photons or neutral pions from interactions.
6. An hadronic calorimeter (HCAL) to assist in muon identification and electron-pion discrimination.
7. A downstream muon tagging system (MUON) to identify and trigger on decay muons and beam muons.

Note that to reduce nuclear interactions the upstream and downstream magnets will also require vacuum pipes.

5.1 Beamline and Experimental Hall

The Meson West beam line (MW) is well suited for our proposed experiment. The MW beamline is not presently assigned to any experiment in the next fixed target run. Furthermore, the differential Cherenkov counter already installed in MW is an important asset for our proposed experiment. In addition, the most recent experiments that have utilized the MW beamline (E706 and E672) have not only received high fluxes of positive and negative secondary particles, but have also received full energy primary proton beams utilizing pinhole collimators installed in the beamline for this purpose. It is our plan to perform the absolute calibration of our spectrometers using a low intensity primary proton beam.

The yield of secondary particles in the MW beam is shown in Fig. 7 as a function of beam momentum when there are 5×10^{11} primary protons on target. The fluxes shown correspond to a beamline configuration in which collimators are set to obtain a beam momentum spread such that $\Delta P/P$ has an rms of 3%. The beam momentum distribution is not Gaussian. The TURTLE Monte Carlo prediction for the momentum distribution at the Cherenkov counter with this beamline configuration is shown in Fig. 8. The predictions for the other beam characteristics (spot size and divergence) are shown in Fig. 9. The beam sizes and divergences are:

Horizontal: 1.1 cm (rms) $\times$0.02 mrads (rms).

Vertical: 0.58 cm (rms) $\times$0.11 mrads (rms).

To estimate the beam fluxes available to the experiment we will assume 5×10^{11} protons on target. We would like to collimate the MW beam so that the momentum spread is similar to the momentum resolution of our proposed upstream spectrometer (T1+EPB-1+EPB-2+T2), which is of the order of 1% (rms). If we collimate to select a beam momentum bite of $\pm 2\%$ then the calculation shown in Fig. 8 implies our particle fluxes will be reduced by a further factor of 2.9 with respect to those shown in Fig. 7. Thus, after collimation at 530 GeV/c we would expect particle fluxes of approximately 5×10^6 per spill (250 KHz) for a positive secondary beam, and 1×10^6 per spill (50 KHz) for a negative secondary beam. Only beam particles within the spatial and angular acceptance of the trigger scintillators will be of use to

the experiment. We must therefore estimate the losses outside of the horizontal and vertical acceptances of our setup. The beam is well contained within the horizontal acceptance. Note that (i) the beam spot at the Cherenkov counter is essentially all contained within ± 2 cm of the beam axis in the horizontal direction, (ii) the momentum bite of $\pm 2\%$ results in an angular spread after the upstream momentum spectrometer of about 0.1 mr which is therefore the dominant contribution to the beam divergence in the decay pipe, and (iii) after the beam propagates 150m the horizontal beam divergence smears the beam spot by only 1.5 cm(rms). In the vertical direction the beam will not be completely contained within the aperture of EPB-4 (the vertical aperture of EPB-4 is about 3 cm). From the distributions shown in Fig. 9 we estimate that the beam size in the vertical direction at EPB-4 will be 1.8cm (rms). We therefore expect about 50% of the beam to be lost outside of the vertical acceptance of our downstream spectrometer. To account for both this vertical acceptance loss and the loss due to the tight momentum selection, we estimate that we must reduce the fluxes shown in Fig. 7 by $2.9 \times 2 = 5.8$. In our estimation of the trigger rates for our experiment we will refer to this factor of 5.8 as a loss due to the geometrical acceptance of our setup.

In Fig. 10 we show the proposed P874 apparatus installed in the MW beamline for the 100 m long decay length configuration. We have assumed that the Cherenkov counter (C) remains at its present position with P874 just downstream of it. The first spectrometer (EPB-1 + EPB-2) and the first 50 m of the decay pipe (D) are within the beam enclosure MW8. This apparatus will sit in the place presently occupied by several beam elements which are shown in Fig. 10 as dashed lines, and which will need to be removed from the enclosure.

The second spectrometer (EPB-3 + EPB-4), the two calorimeters (ECAL and HCAL), plus the muon identifier (MUON), are located at the downstream end of the experimental hall MW9. It would be unrealistic to attempt to find a configuration for a longer decay length. We are presently proposing to use three different decay pipe lengths: 100m, 50m, and 30m. The different length configurations are obtained by moving the downstream spectrometer and detectors. Due to the difference in floor levels between MW8 and MW9, two platforms will need to be built with concrete blocks for the 100 m configuration, and for part of the detectors in the 50 m configuration. For the 50 m configuration the platform will be at the

transition between MW8 and MW9. In the 30 m configuration the entire experiment will be within MW8.

5.2 The Beam Cherenkov Counter

The MW differential Cherenkov counter is a unique device that is capable of good pion-kaon-proton discrimination up to energies of about 530 GeV, and can operate at rates of up to about 10 MHz. A schematic of the 142 foot long counter is shown in Fig. 11. At the exit of the counter light is collected by an 18"-diameter aluminized spherical mirror with a focal length of 106 feet. The Cherenkov optics, consisting of a system of quartz plano-convex spherical lenses and dichroic mirrors (Fig. 12), have been designed to give good pion-kaon separation in spite of the proximity of the π and K light and their chromatic overlap at high energy. Separation in the overlap region is achieved by using lenses, filters, and mirrors to exploit the differences in the wavelengths as well as the directions of photons radiated from the different particle types. The Cherenkov light from traversing pions, kaons, and protons is directed onto three separate rings of high-gain single photoelectron photomultipliers mounted at the upstream end of the Cherenkov counter (Fig. 13). The counter is operated with a Helium radiator at a pressure that is set for each incident beam energy so that the outermost ring of 6 phototubes is illuminated by Cherenkov radiation from traversing pions. The outermost ring is therefore referred to as the π-channel. The middle ring of 6 phototubes, referred to as the p-channel, is illuminated by Cherenkov radiation from traversing protons, and the inner ring of 6 phototubes, called the K-channel, is illuminated by traversing kaons. Each of the three rings of photomultipliers can therefore be used to tag one of the three particle types (pions, kaons, or protons).

Figures 14a, 14b, and 14c show, as a function of the pressure of the Helium radiator, the fraction of particles in an 800 GeV proton beam that result in several phototubes giving signals above threshold for respectively the p-channel, K-channel, and π-channel. The measured pressure curves are well described by a Monte Carlo calculation that (i) includes a full geometrical description of the Cherenkov optics and (ii) takes account of the statistical fluctuations in the number of radiated photons, the phototube efficiencies, and the thresholds on the phototube signals. Thus the performance of the Cherenkov counter is well understood.

Note that the noise level in each of the channels is less than or of order one part in 10^3. A further reduction in noise can be obtained by requiring four, five, or all six phototube signals to be above threshold in the channel of interest.

We have used the Cherenkov counter Monte Carlo program together with the measured energy dependent particle content in the MW beam to calculate pion and kaon tagging efficiencies and mistag fractions for beam momenta of 100, 400, 530, and 600 GeV/c. The results are summarized in Table 7 and shown in Figs. 15, 16, 17, and 18 for respectively π^-, π^+, K^-, and K^+ tagging. At each energy the Helium pressure was chosen to maximize the efficiency for tagging the particle type of interest. The tagging efficiencies and mistag fractions depend upon the number of phototubes required to be above threshold. In the pion tagging calculations Monte Carlo simulated tags were rejected if there were also two or more phototubes above threshold in the p-channel. This requirement is essential to suppress proton contamination for π^+ tagging. A threefold coincidence of π-channel phototubes is predicted to result in a π^- mistag fraction of order 10^{-4} whilst maintaining a tagging efficiency close to 50% for all the beam energies considered. The mistag fraction is larger for π^+ tagging at high energy due to the large proton content of the beam. However, requiring a fourfold coincidence of π-channel phototubes is predicted to result in a π^+ mistag fraction of order 10^{-4} or less whilst maintaining the tagging efficiency above 20%. In all cases the contributions to the pion mistag rates arising from traversing kaons are significantly less than 10^{-4}. Hence, even though the kaon lifetime at high energy is a factor of 0.13 shorter than the pion lifetime, the contamination in the pion decay samples from kaon decays will be less than one part in 10^3.

In summary, with 5×10^{11} protons on the primary MW target our calculations indicate that using the MW differential Cherenkov counter to tag pions in the momentum range 100 GeV/c to 530 GeV/c we should be able to achieve mistag fractions of less than 10^{-4} whilst obtaining tagging rates varying from 15.6 KHz for π^+ tagging at 530 GeV/c to 329 KHz for π^- tagging at 100 GeV/c. These tagging rates are well within the rate capability of the Cherenkov counter. We note that it may be possible to also tag at higher momenta, up to about 600 GeV/c. In this region there are larger uncertainties on the particle fluxes and the performance of the Cherenkov counter.

5.3 Trigger Scintillators and Veto Counters

To trigger on traversing pions and on decaying pions within the acceptance of the upstream and downstream spectrometers we propose to use a system of scintillation counters S1, S2, S3, S4, S5, and S6. We plan to construct the counters from 1/4 inch thick scintillator. The lateral sizes of the upstream trigger counters (S1, S2, and S3) will be small to accept only particles within the vertical acceptance of the magnets that are also within about $\pm 2\%$ of the central beam momentum. The sizes of these counters in our present design are 1cm in the vertical dimension and 2 mm in the bending direction. The trigger counters at the downstream end of the decay pipe will be larger to take account of the finite beam divergence and muon decay angle. In our present design S4 and S5 are 3 cm in the vertical dimension and 10 cm in the bending direction. Finally, S6 will be sufficiently large to cover the entire muon decay acceptance. In our present design S6 is 6 cm in the vertical dimension and 12 cm in the bending direction.

Each trigger scintillator (S1, S2, .. S6) will be surrounded by a veto counter system (V1, V2, .. V6) to reject interactions. Each veto counter system will be comprised of four 1m $\times$ 50cm counters arranged as shown in Fig. 19. This will enable tracks to be rejected if they are accompanied by one or more particles within 50cm of the trigger acceptance. Note that the veto system overlaps the edges of the trigger counters to ensure there are no cracks.

5.4 Upstream Momentum Spectrometer

We have designed the upstream momentum spectrometer to measure the momenta of beam particles with a precision of about 1% at 530 GeV/c. A schematic of the upstream spectrometer is shown in Fig. 20. It consists of two existing 1.5 T external proton beam (EPB) 3 meter long magnets (EPB-1 and EPB-2) powered in series, a system of four tracking chambers (T1) upstream of the magnets, and a system of four tracking chambers (T2) downstream of the magnets.

To obtain a 1% momentum resolution at 530 GeV/c the tracking systems T1 and T2 must measure the track direction in the bending plane with a precision of about 0.05 milliradi-

ans. We propose to accomplish this by making 8 measurements of the track position in the bending direction over a lever arm of 3m upstream of the magnets (T1), and a further 8 measurements of the track position in the bending direction over a lever arm of 3m downstream of the magnets (T2). Each position measurement will have a precision of about 100μm. An analytical calculation of the momentum resolution of the system (T1+EPB-1+EPB-2+T2) at 530 GeV/c gives:

$$\delta p/p = \ (0.85/500) \times p\ \% = \ 0.9\% \tag{26}$$

Members of our collaboration have experience with the construction and operation of drift chambers based on small radius straw tubes, and we therefore propose to use this technology for T1 and T2. The construction of small radius straw tube drift chambers has been extensively developed for the SDC and ATLAS detectors. We do not anticipate difficulties in constructing chambers for our proposed experiment. Figure 21 shows that a spatial resolution of about 130μm has been obtained from an SDC prototype straw chamber which was constructed from 4 mm diameter tubes and operated with a mixture of 50% Argon and 50% ethane. This spatial resolution is adequate for our application. We note however that current draw and aging in the anticipated SDC environment were such that the SDC test was made at relatively low gains ($< 10^5$). We hope to achieve an improved resolution of about 100μm by raising the gain.

The choices of tube radius and length for our application are currently under study. In our initial design we choose 20 cm long 1 cm diameter tubes operated with a mixture of 50% Argon and 50% ethane. This gives a drift time of 100 ns. Each of the tracking systems (T1 and T2) consists of four stations. The 1 cm diameter tubes are arranged vertically in two rows of 4 tubes with the tube centers offset by half a tube diameter to resolve left-right ambiguities, thus providing up to 16 hits per track.

There are a total of 128 channels in the T1 + T2 system. An economical solution for the readout of the straw tubes is provided by the amplifier-discriminator design used for the FNAL E735 experiment. Based on experience at Duke University with the manufacture of these amplifier-discriminator boards the cost is estimated to be less than $10 per channel. The signal arrival times can be digitized using Lecroy 4291 TDCs with 1 ns resolution.

5.5 Downstream Momentum Analyzer

A schematic of the downstream momentum analyzer is shown in Fig. 22. It consists of two EPB magnets (EPB-3 and EPB-4) powered in series with the upstream magnets EPB-1 and EPB-2, a system of tracking chambers (T3) upstream of the magnets, and a system of tracking chambers (T4) downstream of the magnets. The magnets are available and are of the same type we propose to use for the upstream momentum spectrometer. The (T3 + EPB-3+ EPB-4 + T4)-system has been designed to measure track momenta with a precision of about 1% at the highest energies (530 GeV). The analytical calculation of the expected momentum resolution has been confirmed by our results from the GEANT simulation described in a later section of this proposal.

Each tracking system consists of four tracking stations. Thus there are a total of eight stations in the T3 + T4 system. Each station consists of 32 vertical straw tubes and 32 stereo tubes. The vertical tubes are arranged in two rows of 16 tubes with the tube centers offset by half a tube diameter to resolve left-right ambiguities. The stereo tubes are also arranged in two rows with the tube centers offset by half a tube diameter. The stereo angle is $+30^o$ and -30° for alternating stations. Thus the downstream tracking system (T3+T4) consists of 512 tubes.

The total amount of material in the (T3 + T4)-system is 2.0% of a radiation length and 0.75% of an interaction length. Hence the average scattering angle arising from multiple Coulomb scattering is about 0.04 milliradians for 50 GeV/c pions and 0.004 milliradians for 530 GeV/c pions. These angles are of order 0.07% of the bending angle in the downstream momentum analysing magnet, and are therefore negligible.

5.6 Momentum Calibration

We propose to use an 800 GeV/c proton beam to obtain the absolute calibration of the upstream tracking system. Before the magnets are moved into position, the $\int B \cdot dl$ (the integrated magnetic field over the central trajectory) will be measured at several currents including the two currents that correspond to 530 GeV/c and 100 GeV/c operation. The

$\int B \cdot dl$ can be measured as a function of magnet current with a relative accuracy of $\sim 10^{-4}$ and an absolute accuracy of $\sim 10^{-3}$. We assume that the long term stability of the magnet power supplies can be regulated to better than 10^{-3}, and that we will use either a Hall probe or an NMR probe to monitor the field at the magnet poles. After the magnets are in position, the bending angle will be measured for about 10^4 to 10^5 800 GeV/c proton tracks. From the relationship between $\int B \cdot dl$, bending angle, and momentum ($p\theta = 0.03 \int B \cdot dl$), the $\int B \cdot dl$ can be calculated for the magnet currents that correspond to 530 GeV/c running. Assume that we record 10^4 primary proton tracks. The precision of the determination of $\int B \cdot dl$ will then be $1.4\%/\sqrt{10,000} = 0.014\%$. The ratio of the calculated $\int B \cdot dl$ and measured $\int B \cdot dl$ gives the scale factor needed for the absolute momentum calibration. Since the relative accuracy of the $\int B \cdot dl$ measurements at different magnet currents is expected to be about $\sim 10^{-4}$, the true $\int B \cdot dl$ corresponding to other currents can then obtained with this precision.

As a cross check, the $\int B \cdot dl$ can be inferred for several different magnet currents using 800 GeV/c proton trajectories, and the results compared with the direct field integral measurements. We anticipate that the recalibration of the spectrometer with 800 GeV/c protons may be necessary periodically. Although the calibration of the downstream spectrometer system is not as important as the upstream system, we note that once the upstream spectrometer is properly calibrated it is straightforward to transfer the calibration to the downstream momentum analyzer using, for example, 530 GeV/c secondary particles.

5.7 Calorimeters

Calorimetry is required in our proposed experiment not only to assist in the discrimination between charged pions and muons, but also to reject electron contamination in the beam, and to record the presence of any photons or other neutral particles accompanying the charged track that might indicate either bremsstrahlung or a nuclear interaction in the vacuum pipe walls or windows, track chamber material, or magnet walls. Hence both electromagnetic and hadronic calorimeters are required. We have simulated pions traversing our experimental setup using the GEANT Monte Carlo program, and find that at the calorimeter face all decay muons are contained within an envelope that is 5cm wide in the bending plane and 4

cm wide in the orthogonal co-ordinate. Hence the lateral dimensions of the calorimeters in our experiment can be quite small.

Several prototype calorimeters have recently been built which are of the appropriate size and are available for our proposed experiment. We propose to (i) construct a small electromagnetic calorimeter for our experiment using materials from a prototype electromagnetic calorimeter built for the CDF plug calorimeter upgrade, and (ii) use an existing high-pressure gas-ionization hadronic calorimeter built as part of the SSC detector *R&D* program. We are also considering the alternative high pressure gas option for the electromagnetic calorimeter that is described in Appendix 2.

5.7.1 Electromagnetic Calorimeter

We propose to use material from existing calorimeter prototypes to construct a lead - scintillator electromagnetic calorimeter suitable for our experiment. The calorimeter will use the tile/fiber technique developed for the CDF plug calorimeter upgrade. In our provisional design the calorimeter that we propose to build has a cross-section of 22×22 cm^2, a depth of $42X_0$ (2 interaction lengths), and will be constructed using 1 cm thick lead absorber plates and 6mm thick scintillator tiles with a cross-section of 22×22 cm^2. To obtain good e - $\pi^{\pm}$ discrimination the calorimeter will be segmented into 4 depth segments, each read out by a separate phototube. The segmentation will be $5X_0$ (3 tiles), $12X_0$ (7 tiles), $5X_0$ (3 tiles), and $20X_0$ (11 tiles). Thus there will be a total of 24 tiles. Experience gained from construction and testing the CDF prototype tile/fiber calorimeter enables us to reliably estimate that the light yield will be 150 pe/GeV. The expected energy resolution is $22\%/\sqrt{E}$. A minimum ionizing track will deposit 9 - 10 photoelectrons in the $5X_0$ samples. Hence all longitudinal samples will be sensitive to muons. This sensitivity will assist in pion/muon identification.

5.7.2 Hadronic Calorimeter

We propose to use an existing high-pressure gas-ionization hadronic calorimeter that was built as part of the SSC detector *R&D* program. A detailed description of the calorimeter can be found in Ref. [10]. A schematic of the calorimeter is shown in Fig. 23. The calorimeter

consists of 14 modules. A schematic of one module is shown in Fig. 24. Each module has a cross-section of 10×10 cm^2, is 3m long, and contains about 13 interaction lengths of steel. The modules are constructed from 64 straight tube ionization chambers (Fig. 25) which have a 1.6 mm gas gap, are 3m long, and are operated with a gas mixture of 95% Ar + 5% CH_4 at a pressure of 100 atmospheres. Thus the 14 calorimeter modules are constructed from a total of 896 ionization tubes.

The calorimeter is equipped with the low impedance preamplifiers described in Ref. [10]. Each input transistor is connected to two calorimeter tubes. Each amplifier has 8 input transistors and collects signals from an array of 4×4 tubes. There are four output signals from each module, and therefore a total of 56 output signals which are digitized by a 2249A ADC. The electronic noise of the preamplifiers corresponds to 4 GeV. We therefore expect the calorimeter to be sensitive to hadronic showers with energy in excess of about 10 GeV.

The calorimeter was tested at the CERN - SPS in July 1993 with pion and electron beams in the energy range from 10 to 100 GeV (Ref. [10]). The tubes were operated at a high voltage of 1.2 kV. The observed signals had a full width of about 80 ns. The measured response of the calorimeter to electrons is seen to be linear whilst its response to hadrons increases with energy slightly faster than linearly (Fig. 26). This is due to the well-known decrease of the e/h response with increasing energy. This nonlinear behavior is well reproduced by Monte Carlo simulations. The measured value of the e/h response is 1.3 for a 50 GeV beam energy. The measured pulse-height distribution for a 75 GeV pion beam is shown in Fig. 27. The spectrum exhibits two well separated peaks corresponding to incident pions and muons. The width of the pion peak is the result of intrinsic signal fluctuations, electronic noise, and fluctuations in the lateral shower leakage. To obtain the intrinsic calorimeter resolution the electronic noise was quadratically subtracted and the results corrected for lateral shower leakage using a Monte Carlo simulation. The final results for three incident beam angles (0.9^o, 2.9^o and 9.1^o) are shown in Fig. 28a. Fitting the combined experimental pion data yields:

$$\sigma_E/E \;=\; (70 \pm 12)\%/\sqrt{E} \;\oplus\; (7.4 \pm 1.2)\%. \tag{27}$$

The constant term can be reduced offline by using an e/h compensation software algorithm. The calorimeter energy resolution after applying this compensation procedure is shown in

Fig. 28b. The best fit in this case does not include any constant term:

$$\sigma_E/E \;=\; (64 \pm 6)\%/\sqrt{E}. \tag{28}$$

However, because of statistical errors, we cannot exclude a constant term of less than 3%.

Testbeam measurements have only been performed up to energies of 100 GeV. In Fig. 29 we show a Monte Carlo prediction for the response of the calorimeter to 500 GeV pions. The simulation includes the detailed calorimeter geometry. No e/h compensation procedure was used. There is no evidence for a significant distortion in the spectrum due to lateral shower leakage. The Monte Carlo simulation for 500 GeV pions indicates that the limited transverse size of the hadronic calorimeter results in a leakage of about 8% of the shower energy. The fluctuations of energy losses depend on incident hadron energy, the fluctuation r.m.s. is equal to $(6.5 \pm 0.6)\%$ at 100 GeV and slowly decreases with increasing energy. As a result we expect that after applying a software e/h compensation algorithm the energy resolution of the calorimeter will be about 6% for 500 GeV pions.

In our proposed experimental setup, to ensure that the amount of material upstream of the muon tagger is uniform over the active surface of the tagger, we would either construct two additional calorimeter modules to provide a square matrix of 4×4 calorimeter modules, or alternatively we would place iron absorber in the positions of the missing modules. Finally, to obtain the best intrinsic calorimeter energy resolution the HCAL would be positioned such that its axis was 3° from the beam direction.

5.8 Muon Identification

To be able to measure the pion lifetime with a precision of 0.1% the experiment must:

- Identify high energy muons with an efficiency known to better than 0.1%.
- Identify decay muons with a rejection against beam muons faking a decay muon of greater than 10^3, which will require a precise momentum determination at the upstream and downstream ends of the decay region.

- Identify decay muons with a rejection against beam pions faking a decay muon of greater than 10^5, which in addition to the rejection based on the momentum measurement will require a muon tagging system to obtain a further rejection of 100.
- Trigger on muons with a factor of 1000 rejection against pions or better (note that pions which do not decay will outnumber decay muons by a factor of about 300 for a 100 m decay length).

To achieve these goals we propose to supplement the muon identification capability of the ECAL and HCAL with the addition of a muon tagger (MUON) downstream of the HCAL. The design of the muon tagger has been guided by our understanding of the characteristics of hadronic shower punchthrough at high energies. Several publications [11, 12] have characterized hadronic shower punchthrough for different incident hadrons in terms of punchthrough probabilities as a function of penetration depth in iron absorbers. More detailed studies [13, 14] of the momentum and angular distributions of punchthrough muons have been performed recently by the RD5 Collaboration at CERN. These studies have been limited to incident hadron energies up to 300 GeV and total detector depths of about 30 nuclear interaction lengths (λ). For incident hadron energies between 10 and 300 GeV, curves showing the punchthrough probability vs. penetration depth are characterized by two distinct regions. For depths less than about 3 m iron equivalent, the curves have steep slopes which represent the absorption of the hadronic component of showers. For depths greater than 3 m iron equivalent, the curves flatten out. This represents the ranging out of penetrating punchthrough muons produced as a component of the hadronic shower. In our proposed experiment, the transition between the two regions occurs approximately at the interface between the hadronic calorimeter and the muon tagger. The data in Ref. [14] show that 300 GeV positive and negative pion showers have a total punchthrough probability of about 0.005 at a depth of 5.29 m iron equivalent. Punchthrough muons are generally low in energy, a 30 GeV muon being 100 times less probable than a 5 GeV muon. Higher energy muons are more forward peaked than lower energy muons. The angular distributions for both higher and lower energy muons are wider than they would be if multiple scattering were the only process affecting the distributions, reflecting the hadronic processes in the calorimeter.

With the muon tagger described below, we anticipate that the total depth of the ECAL + HCAL + MUON system will be 45 λ. This should facilitate the separation of muons

from pions for energies up to 530 GeV or beyond, and provide the capability of triggering on muons with a pion rejection factor of about 1000 or better.

5.8.1 The Muon Tagger

The muon tagger (MUON) has been designed to provide a muon trigger and, together with the ECAL and HCAL, provide muon identification offline. Figure 30 shows a preliminary design for the muon tagger. The muon tagger is located downstream of the hadronic calorimeter and is centered on the direction of the pion beam after deflection through the downstream momentum analyzer. The muon tagger consists of 12 stations of iron absorber each followed by a scintillation counter, and three planes of proportional tubes. The thickness of each absorber station is 42 cm, which is equivalent to 2.5 λ. This gives a total absorber thickness of 500 cm (30 λ). The 2.5 λ thick absorber stations will be built from 0.3 λ thick iron plates. This modular design will allow us to modify the absorber thickness per station and the total number of stations, scintillation counters, and proportional tube planes, should we need to optimize the sampling of the muon tagger as we evaluate its performance during data taking.

In our preliminary design of the muon tagger each of the scintillation counters consists of a single 1.9 cm $\times$ 40 cm $\times$ 40 cm piece of polystyrene scintillator viewed by a trapezoidal light guide and a photomultiplier tube. In addition there are three planes of horizontal and vertical proportional tubes at the following positions: in front of the muon tagger, at a depth of 15 λ, and after the last station of the muon tagger. The proportional tube planes have a transverse granularity of 2.5 cm and therefore provide a fine-grained view of tracks as they travel through the tagger. A proportional tube plane will consist of 16 horizontal and 16 vertical tubes, making a total of 96 tube channels for the three planes.

The lateral size of the muon tagger is 40 cm $\times$ 40 cm, which is approximately the same as the hadronic calorimeter and is sufficient to ensure that decay muons will penetrate the entire depth of the tagger. Neglecting multiple scattering in the ECAL and HCAL, with a pion beam of 530 GeV the highest energy decay muons of 530 GeV strike the muon tagger face at its center with normal incidence. The lowest energy decay muons of 300 GeV bend 4 mrad more than the highest energy muons in the downstream momentum analyzer. As

stated in Section 5.7, the lowest energy muons are contained within an envelope 5 cm wide in the bending plane at the face of the ECAL. This envelope will be about 7 cm wide at the MUON face and about 9 cm wide at the exit of the muon tagger, again neglecting multiple scattering. Including multiple scattering does not affect the containment of decay muons in the muon tagger. As an example, when a 100 GeV muon traverses all three detectors (ECAL, HCAL and MUON) it is deflected a lateral distance of 1.8 cm (rms) at the exit of the muon tagger.

In order to achieve the third particle identification goal listed at the beginning of this section, the combined ECAL + HCAL + MUON system must be able to reject pions with a factor of 100 or better. Note that the combined absorber thickness of the electromagnetic calorimeter (2 λ), the hadronic calorimeter (13 λ) and the muon tagger (30 λ) is 45 λ. A high energy muon traversing the three detector elements will deposit about 12 GeV of energy through ionization, 0.5 GeV in the ECAL, 3.4 GeV in the HCAL, and 7.9 GeV in the MUON. Since every pion will initiate a hadronic shower, we believe that a pion rejection factor of 100 can be readily accomplished with cuts on the energy measured in the HCAL and the penetration depth in the MUON. Note that the punchthrough probability of 0.005 for 300 GeV muons at about 5 m iron equivalent is by itself an encouraging number. Most of the punchthrough events at this depth yield low energy muons which will range out before the end of the muon tagger. Remaining punchthrough muons at the end of the muon tagger will have a large angular divergence which can be seen with the last proportional tube station.

5.8.2 Triggering on Muons

At the trigger level we need to achieve about a factor of 1000 rejection against pions, and accomplish this with a muon efficiency that is known to $\pm 0.1\%$. We propose to achieve this by using the signals from the muon tagger scintillators to form a muon trigger. A component of this trigger might be to require that one of the last three scintillator counters in the muon tagger is above threshold. Note that there will be 7m of iron equivalent upstream of these scintillators which should by itself be sufficient to achieve the desired rejection against pions. In addition, signals from the other scintillators in the muon tagger can be used to increase the rejection against pion punchthrough. As an example of a possible trigger, consider first

a coincidence of any 9 out of the 12 muon tagger scintillators, i.e. a trigger where any 3 scintillators are allowed not to fire. Let ϵ be the efficiency for a minimum ionizing signal to fire an individual counter. The photomultiplier gains and discriminator thresholds can be adjusted so that ϵ is greater than 95% and approximately the same for all counters. For a minimum ionizing particle which passes through all 12 counters, the overall efficiency for the above trigger is:

$$\epsilon_{tot} = \epsilon^n + n\epsilon^{n-1}(1-\epsilon) + \frac{n!}{(n-2)!2!}\epsilon^{n-2}(1-\epsilon)^2 + \frac{n!}{(n-3)!3!}\epsilon^{n-3}(1-\epsilon)^3 \quad (29)$$

where n = 12. The first term represents the case where each of the 12 counters fire, the second term represents the 12 cases where only one counter does not fire, etc. For $\epsilon = 0.95$, the overall efficiency is 99.78% with the four terms contributing 54.04%, 34.13%, 9.88%, and 1.73%, respectively. For $\epsilon = 0.98$, the overall efficiency is 99.99%. If in addition to 9 out of 12 muon tagger scintillators firing we also require that one of the last 3 scintillators fires then the muon efficiency is decreased by only 1 of the 220 3-miss combinations described by the fourth term in the preceeding equation. Thus we believe that we can achieve a rejection of 1000 against pions at the trigger level whilst maintaining good muon triggering efficiency.

Finally, we consider other sources of inefficiency in our muon identification system. A small fraction of the muons will suffer a substantial energy loss in the ECAL, HCAL and MUON due to e^+e^- pair production, bremsstrahlung, and photonuclear interactions. The first two processes are comparable in probability and lead to localized electromagnetic showers accompanying the minimum ionizing muon track. Photonuclear interactions are less likely, but can lead to much larger energy loss in the detectors which will reduce the trigger efficiency and offline reconstruction efficiency for such muons. A GEANT study simulating the energy loss of 530 GeV muons and pions in the absorber material of the detectors shows that 0.3% of the muons deposit a large amount of energy in the HCAL which is within the limits of the measured energy distribution for pions, potentially making these muons indistinguishable from pions. In order to accomplish the goal of knowing the efficiency for muons to 0.1%, the above 0.3% muon inefficiency will need to be determined with about 30% accuracy. We are considering several schemes for this determination. The preferred scheme is to produce a pure muon beam by closing a collimator and beam stop upstream of

the experiment. We estimate that a sufficiently precise measurement of the muon efficiency can be obtained by running in this mode for about 2 days. A second scheme is to collect a data sample of muons with the muon tagger placed in front of the ECAL and HCAL.

We conclude that with the proposed ECAL + HCAL + MUON system we should be able (i) to identify decay muons with a high efficiency which can be determined with the required precision, and (ii) obtain the required rejection against pions both offline and at the trigger level.

5.9 Data Acquisition

We propose to use a UNIX based workstation for our data acquisition. The exact system will be subject to the recommendation of the Computer Division. A candidate system could be the SGI Indy connected to CAMAC with a SCSI Jorway interface which has been shown to be able to read CAMAC at 500 kb/s with a readout latency of 800μs. A summary of the total number of electronics channels to be read out and the estimated data size is given in Table 8. Adding a 25% contingency to allow for additional information to be added to the event record we estimate that the event record size will be about 1 kb. Therefore, assuming a maximum of 500 kb/s to tape with 800μs latency, our maximum data taking rate will be about 360 Hz. Note that with the estimated trigger rates shown in Table 9 a maximum data taking rate of 360 Hz will only limit the rate at which we record events at 100 GeV. If the measured trigger rates turn out to be higher than expected then we could obtain a higher data taking rate by using a VME based system with a VME-CAMAC interface. This would reduce the trigger latency to 2μs and increase the maximum data rate to 500 Hz.

5.10 Triggers, Data Rates, and Beam Requirements

The triggers will use (a) the Cherenkov counter information (C_π, C_K, C_p) to distinguish between pions, kaons, and protons, (b) the scintillators S1, S2, S3, S4, and S5 to define an incident track of the correct momentum and direction, (c) the scintillator S6 to select tracks within the acceptance of the calorimeters and muon tagger, (d) the veto counter systems V1,

V2, V3, V4, V5, and V6 to reject interacting particles, and (e) the muon tagger information MUON to select muon candidates. To select pion decays and determine the incident pion flux we will need (i) a pion decay trigger (S1.S2.S3.S4.S5.S6.MUON) to record $\pi \rightarrow \mu\nu$ decays and to record the muon contamination in the beam, and (ii) a traversing pion trigger (C_π.S1.S2.S3.S4.S5.S6) to count the total number of incident pions during pion data taking, and to record them with a prescale factor of about 1000.

Constraints on the trigger and data taking rates arise from (a) the number of 800 GeV protons available for the MW primary target, which we will take to be 5×10^{11} per spill, and (b) the maximum rate at which events can be recorded to tape, which we take to be 360 Hz. The two pion triggers would be run simultaneously, and hence the maximum trigger rate for the individual triggers is 180 Hz.

In Table 7 a summary is given of the calculated Cherenkov tagging rates that correspond to 5×10^{11} protons on the MW primary target per spill. To estimate the trigger rates we need to calculate (1) the fraction of the tagged pions that are within the geometrical acceptance of the trigger counters and (2) the fraction of the tagged particles that decay in the decay region of the experiment. This information is summarized in Table 9. We can now estimate the beam time required to make a precision measurement of the π^+ and π^- lifetimes at high energy. We will assume that we can write to tape a maximum of 3600 events per spill, that there are 720 spills per day (50% accelerator efficiency), and that each measurement requires 8 hours of setup time to tune the beam optics, Cherenkov, magnet currents, and trigger. We will also assume that in addition to measurements at the highest practical beam energy (530 GeV) we will require data at one lower energy, which we have provisionally taken to be 100 GeV. Estimates of the beam time required to measure the lifetimes at 100 GeV/c and 530 GeV/c are summarized in Table 10. Each lifetime requires measurements at two values of decay length to enable corrections for end effects. We believe that to provide some additional constraints on systematic effects we will also need measurements at a third decay length. We therefore propose to measure the decay fractions at 100m, 50m, and 30m. With the data samples listed in Table 10 the statistical precision of our measurements would be 0.1%.

We estimate that to complete our π^+ and π^- lifetime measurements at 100 GeV/c and

530 GeV/c will require 5×10^{11} protons on the primary MW target for a total of 1734 hours (10 weeks) with a decay length of 100m, a further 1221 hours (7 weeks) with a decay length of 50m, and 674 hours (4 weeks) with a decay length of 30m. These time estimates include a factor of 0.5 for the accelerator efficiency and 8 hours per measurement setup time.

5.11 Offline Requirements

The total number of pion decays that we propose to record at each decay length is summarized in Table 10. With an event size of 1 Kbyte, the total dataset size would be 1 Kbyte $\times$19.8 million events = 19.8 Gbytes. In addition we will plan to record an equal number of traversing pions. Therefore, we estimate that the total pion decay plus traversing pion dataset size will be 39.6 Gbytes. Allowing an additional factor of two to take account of background contributions and calibration samples, we estimate that our total dataset size will be 80 Gbytes. Thus our mass storage needs will be modest. Furthermore event reconstruction will be simple, and we would plan to reconstruct our full data sample using a 50 MIP workstation or equivalent.

6 GEANT Simulation Results

We have used the GEANT Monte Carlo program to simulate the response of the tracking and triggering elements of our proposed experiment when 530 GeV/c pions are incident at the upstream end of the Cherenkov counter. In our simulations the beam spot size at the Cherenkov counter was taken to be 1mm $\times$ 1cm with a momentum spread $\Delta p/\ p = 1\%$. The GEANT calculation includes a description of the material of the Cherenkov counter, all vacuum chamber windows, and the trigger and veto scintillators. Also included are the magnetic fields at the upstream momentum selector and downstream momentum analyzer, and the downstream tracking elements which have spatial resolution functions that are assumed to be Gaussian distributions with rms widths of 100μm. We have generated samples of 250000 simulated pions incident on our experimental setup where the decay volume length is 100m, and a further 250000 pions with a decay volume length of 50m.

Figure 31 shows for the simulated events the distribution of reconstructed track momenta at the downstream momentum analyzer. The distributions are shown for decay pipe lengths of (a) 100m and (b) 50m. To enter the plots the simulated tracks must deposit energy in the trigger scintillators, and no energy in the veto counters. The resulting momentum distributions are reasonably well described by Gaussian distributions with widths that indicate that the momentum resolution is better that 1%. The simulated measured momentum distributions are also shown in Fig. 32 with logarithmic scales and over a wider range of momenta. In addition to the Gaussian peak centered on the beam momentum there are also long flat tails at lower momentum which can be identified with muons from pion decay. Indeed, we have used the fractions of the simulated tracks that populate the low momentum part of these distributions to compute the pion lifetime. Within the statistical precision of the Monte Carlo samples we recover the correct result. Finally, in Fig. 33 we show the distributions of decay positions along the decay volume for the two decay volume lengths. As expected end effects arising from decays within the magnetic field volumes of the setup contribute to the effective lengths of the decay volumes. The effective lengths are therefore a little longer than 100m and 50m. However, within the statistical precision of the Monte Carlo sample, the end effect contributions are seen to be the same for the two decay volume lengths, so that the difference in effective decay lengths is just 50m.

7 Cost

A summary of the expected costs of the proposed experiment is shown in Tables 11, 12, 13, and 14. At this stage the estimated costs are preliminary.

Table 11 shows estimated costs for the removal and installation of the major pieces of hardware in the beam enclosure MW8 and the experimental hall MW9. We have assumed that vacuum equipment for the EPB magnets and the decay pipe is existing, and that since we are removing some of the beamline magnets, there will be a 500 kW Transrex power supply available and already in place. Only the MCM 500 cables for the run between EPB1/2 and EPB3/4 are required.

Table 12 summarizes our estimates of the costs for the different components of our pro-

posed detector. We have assigned a division of responsibility for these costs based on experience and practicality. It is our plan to use as much recycled material as possible. We expect all scintillator and phototubes to come from existing sources at Fermilab and within the collaboration. At present we have not decided on the best location for the electronics. We assume that the counting room at the north end of the MW building could be used, and have estimated cable costs for that location. It is likely that existing cables could be utilized and hence most of the cable cost avoided.

Table 13 gives a very preliminary list of electronics and DAQ equipment needed (note that a summary of the total number of electronics channels for each detector system is given in Table 8). We have listed specific model numbers for identification purposes only. Our expectation is that only a few new purchases will be required. In the case of DAQ equipment the actual items will depend on the direction that the Computing Division will indicate for our efforts.

Finally, an overall summary of the costs is given in Table 14.

8 Schedule

Our schedule for the installation and data taking of the proposed experiment follows closely the Fermilab draft schedule dated January 1995. That schedule divides the next fixed target running into 4 periods, each of approximately 4 months in duration.

Our goals for the first of the 4 running periods would be to (a) measure the beam characteristics and performance of the Cherenkov counter at 530 GeV/c and 100 GeV/c with the beamline tuned for our experiment, (b) measure the trigger rates for the upstream part of the detector (Cherenkov plus upstream momentum selector), (c) with a low intensity primary proton beam check that we can calibrate the upstream momentum spectrometer with the desired precision, and (d) with a muon beam (collimators closed) measure the muon tagging efficiency for the combined ECAL-HCAL-MUON system, and (e) debug and commission most of our readout and DAQ system. To achieve these goals we estimate that we will need an intensity of 5×10^{11} protons of target for about 4 weeks. For this first running period

we would plan is to install (i) the upstream momentum selector (T1+EPB-1+EPB-2+T2), (ii) the trigger and veto counters 1 through 3, and (iii) the downstream detector components (ECAL, HCAL, and MUON). We would not install the decay pipe or the downstream momentum analyzer at this stage, and the ECAL, HCAL, and MUON would be installed immediately after the upstream momentum selector.

For the second running period we would install the remainder of the experiment (the vacuum decay pipe, the downstream momentum analyzer, and remaining trigger and veto counters) in the 30m decay pipe configuration. The ECAL, HCAL and MUON detectors would be moved to this configuration. Our data taking would require positive and negative secondary beams at 530 GeV/c and 100 GeV/c, together with some low intensity primary proton running for calibration, and some muon beam (collimator closed) running for systematic studies of the muon tagging efficiency. An intensity of 5×10^{11} protons of target will be required for about 4 weeks. We have chosen the 30m length as it requires the shortest running time and allows for more setting up and debugging contingency time. If data taking proceeds smoothly we could attempt to switch over to a 100m decay length geometry.

For the third running period we will complete data taking at 530 GeV/c and 100 GeV/c with the 100m decay length geometry. We will require 5×10^{11} protons on target/spill for a total of 10 weeks. We would also need some low intensity primary proton running for calibration, and some muon beam running to check the muon tagging efficiency.

For the fourth running period we will concentrate on data taking at the remaining geometry of 50 m decay length. We will require 5×10^{11} protons on target/spill for a total of 7 weeks. We would also need some low intensity primary proton running for calibration, and some muon beam running to check the muon tagging efficiency.

The schedule above should be flexible enough so that further running at any of the 3 geometries and 2 energies could be pursued if required. Should we decide that interesting precision high energy measurements of the $K^{\pm}$ lifetime are also practical with our experimental setup we would take kaon tagged data in parallel with our pion data taking.

9 Summary

During the coming Fermilab fixed target run we propose to make precise measurements of the π^+ and π^- lifetimes at the highest energies that are practical at Fermilab. In particular, we propose to measure the π^+ and π^- lifetimes at 530 GeV and 100 GeV with precisions of about 0.1%. We plan to determine the lifetimes by measuring the fraction of pions that decay whilst traversing 100m, 50m, and 30m long decay lengths. Precise momentum measurements at the upstream and downstream ends of the decay region together with good muon identification will enable pion decays to be cleanly identified. We estimate that the experiment will require 5×10^{11} protons on target for a total of 25 weeks during the coming fixed target running periods. Finally, we note that in addition to our proposed pion lifetime measurements we may also be able to make precise measurements of the K^+ and K^- lifetimes at high energy. This is presently under study. Within the framework of some specific models we expect our proposed measurements to be sensitive to a Lorentz non-invariant or CPT violating interaction at a distance scale of order 10^{-18} cm, or a Lorentz non-invariant or CPT violating component of the normal weak interaction Hamiltonian at the level of one part in 10^{10}.

References

[1] F. Lobkowicz et al; Phys. Rev. Lett. 17, 548 (1966).

[2] D.I. Blokhintsev, Phys. Lett. 12, 272 (1964).

[3] L. B. Redei, Phys Rev. 145, 999 (1966).

[4] L.E. Lundberg and L.B. Redei, Phys. Rev. D3, 1051 (1971).

[5] N. Grossman et al; Phys. Rev. Lett. 59, 18 (1987).

[6] D. Newman et al; Phys. Rev. Lett. 40, 1355 (1978).

[7] P.S. Cooper et al; Phys. Rev. Lett. 42, 1386 (1979).

[8] H.B. Nielsen and I. Picek, Phys. Lett. 114B, 141 (1982).

[9] R. Huerta and J.L. Lucio M; Phys. Lett. 131B, 471 (1983).

[10] S.L. Bagdasarov et al; Nucl. Instr. and Meth. A351 (1994) 336.

[11] F.S. Merritt et al; Nucl. Instr. and Meth. A245 27 (1986).

[12] P.H. Sandler et al; Phys. Rev. D42 759 (1990).

[13] "Measurement of Hadronic Shower Punchthrough in a 3 Tesla Magnetic Field", C. Albajar et al; (CERN RD5 Collaboration), to be submitted to Zeitschrift fur Physik C, April 1995.

[14] "Measurement of Momentum and Angular Distribution of Punchthrough Muons at the RD5 Experiment", C. Albajar et al; (CERN RD5 Collaboration), to be submitted to Zeitschrift fur Physik C, April 1995.

[15] R. Huerta-Quintanilla and J.L. Lucio M; Phys. Lett. 124B, 369 (1983).

[16] E. Fischbach et al; Phys. Rev. D32, 154 (1985).

[17] J. Bailey et al; Nucl. Phys. B150, 1 (1979).

[18] Particle Data Group; Phys. Rev. D50, 1173 (1994).

[19] W.T. Ford et al; Phys. Rev. Lett. 18, 1214 (1967).

[20] G. Zech et al; Nucl. Phys. B124, 413 (1977).

[21] M. Bourquin et al; Nucl. Phys. B241, 1 (1984).

[22] K.B. Luk et al; Phys. Rev. D38, 19 (1988).

[23] M. Jakobson et al; Phys. Rev. 81, 894 (1951).

[24] J. Ashkin et al; Nuovo Cimento 16, 490 (1960).

[25] K.F. Kinsey et al; Phys. Rev. 144, 1132 (1966).

[26] M. Eckhause et al; Phys. Lett. 19, 348 (1965).

[27] M.E. Nordberg et al; Phys. Lett. 24B, 594 (1967).

[28] A.F. Dunaitsev et al; Sov. J. Nucl. Phys. 16, 292 (1973).

[29] H. Anderson et al; Phys. Rev. 119, 2050 (1960).

[30] R. Durbin et al; Phys. Rev. 88, 179 (1952).

[31] V.I. Petrukhin et al; SJNP 9, 327 (1969).

[32] D.S. Ayres et al; Phys. Rev. D3, 1051 (1971).

[33] Albrecht et al; Phys. Lett. B199, 580 (1987).

[34] Browman et al; Phys. Rev. Lett. 33, 1400 (1974).

[35] H.W. Atherton et al; Phys. Lett. 158B, 81 (1985).

[36] R.J. Ott and T.W. Pritchard, Phys. Rev. D3, 52 (1971).

[37] Clayton et al; Nucl. Phys. B95, 130(1975), Poulard et al; Phys. Lett. 46B, 135 (1973).

[38] Baltay et al; Phys. Rev. D9, 49 (1974).

[39] R.J. Hemingway et al; Nucl. Phys. B142, 205 (1978).

[40] V.B. Braginskii and V.I. Panov, JETP 34, 463 (1972).

Appendix 1: Existing Limits on the Nielsen and Picek Parameter δ

In addition to modifying the time dilation formula for particle decays at high energy the Lorentz non-invariant interaction of the Nielsen and Picek model is expected to give rise to other observable effects, which have been discussed in the literature. Resulting limits on δ are listed in Table 5. Some details are given in the following.

Huerto and Lucio point out [15] that in contrast to the muon lifetime, the Michel parameter ρ is sensitive to δ:

$$\rho = \frac{3}{4} - \frac{1}{2}\delta \,. \tag{30}$$

Inserting into this expression the particle data book value $\rho = 0.7518 \pm 0.0026$ we obtain $\delta \leq 0.010$ (at 2σ). This is clearly not competitive with the high energy lifetime measurements.

Fischbach et al. [16] point out that the Lorentz non-invariant effects that arise in the Nielsen and Picek model should result in a composition dependence in the gravitational acceleration of a test mass. This effect is due to the modification of the weak interaction contributions to the nuclear binding energy that are implied in the Lorentz non-invariant model. Such an effect has been looked for in the Eötvos experiments. However the limit on the parameter δ reported from these measurements [16] is relatively modest ($\delta < 2.2 \times 10^{-3}$). The Eötvos measurements do not therefore appear to be competitive with the high energy lifetime measurements.

A better result has been obtain by Fischbach et al from a consideration of the lack of measured energy dependence in the $K_L - K_S$ mass difference. The energy dependence of the mass difference Δm is given by:

$$\Delta m(\delta) = \Delta m \, (1 + \frac{4}{3}\delta\gamma^2) \,. \tag{31}$$

Using this, Fischbach et al obtain $\delta < 1.3 \times 10^{-5}$. Again, this is not competitive with the expected sensitivities of our proposed measurements.

Finally, it has been pointed out to us that in addition to the datasets referred to in Table 5 there also exists new higher energy hyperon data samples. Although lifetime results are not yet available from these new datasets we can estimate their potential sensitivity to a Nielsen and Picek deviation from the time dilation formula. As an example consider the E761 sample of Σ^+ decays at 375 GeV/c and assume that this data sample results in a

very precise lifetime measurement so that the uncertainty on determining the deviation Δ is dominated by the uncertainty on the low energy lifetime measurements (0.5%). Under the assumption that $c_2 = 1$, a two standard deviation difference in δ from zero would correspond to a value $\delta = 1.0 \times 10^{-7}$. Note that this value of δ is significantly smaller than any value excluded by the limits derived from the published measurements summarized in Table 5. Nevertheless, the potential sensitivity of the E761 Σ^+ lifetime measurement is still almost three orders of magnitude less than the sensitivity of our proposed $\pi^\pm$ lifetime measurements. Thus we conclude that within the framework of the Nielsen and Picek model our proposed high energy pion lifetime measurements would be several orders of magnitude more sensitive to a non-zero δ than any existing lifetime measurements.

Appendix 2: An alternative electromagnetic calorimeter

As an alternative to the electromagnetic calorimeter described earlier in this proposal we are also considering using a high-pressure gas-ionization electromagnetic calorimeter. This calorimeter consists of 127 tube ionization chambers arranged in a hexagonal matrix. The hexagon has sides of length 6.8 cm and is 73.5 cm deep (23 X_0). The calorimeter has an active area which is hexagonal with an apex-to-apex separation of 11 cm. The drift tubes are constructed from 9.5 mm diameter stainless steel tubes in which there is a central 0.4 mm diameter copper rod. The drift tubes are bent on a wavy form to avoid channeling effects. The tubes are operated with a gas mixture of 95% Ar and 5% CH_4 at a pressure of 100 atmospheres.

The calorimeter was tested at the CERN - SPS in 1994 with electron beams in the energy range from 10 to 70 GeV. The full signal width using a 1.5 KV potential across the 2mm drift gap was measured to be about 70 ns. In the energy range from 20 to 70 GeV the calorimeter is linear to within 0.5%. The measured energy dependence of the calorimeter EM energy resolution is given by:

$$\sigma(E)/E \;=\; a/\sqrt{(E)} \oplus b \tag{32}$$

where a = $(32.0 \pm 1.6)\%$ and b = $(2.9 \pm 0.3)\%$. Therefore the energy resolution at 500 GeV is expected to be 3.2%. The internal electronic noise of the amplifiers corresponds to 0.3 GeV r.m.s.

Particle	E (GeV)	γ	τ/γ (Secs)	Precision (%)	Ref.
$\mu^{\pm}$	3.1	29.3	$2.195(1) \times 10^{-6}$	0.05	[17]
$\tau^{\pm}$	45.0	25.3	$2.956(31) \times 10^{-13}$	1.0	[18]
$\pi^{\pm}$	1.8	12.9	$2.667(24) \times 10^{-8}$	0.9	[1]
$K^{\pm}$	3.0	6.1	$1.221(11) \times 10^{-8}$	0.9	[19]
K_S^0	375.	754.	$8.83(60) \times 10^{-9}$	6.8	[5]
Λ^0	16.5	14.8	$2.7(2) \times 10^{-10}$	7.4	[20]
Ξ^0	14.0	10.7	$2.78(4) \times 10^{-10}$	1.4	[20]
Ξ^-	131.	99.1	$1.652(51) \times 10^{-10}$	3.1	[21]
Ω^-	198.	118.	$8.11(37) \times 10^{-11}$	4.6	[22]

Table 1: Compilation of existing high energy lifetime measurements for weakly decaying particles.

Paper	Ref	Momentum	Lifetime (τ/γ) (10^{-8} secs)
World Average	[18]	0	2.6030 ± 0.0024
Jakobson (1951)	[23]	0	2.54 ± 0.11
Ashkin (1960)	[24]	0	2.546 ± 0.032
Kinsey (1966)	[25]	0	2.640 ± 0.008
Eckhause (1965)	[26]	0	2.602 ± 0.004
Nordberg (1967)	[27]	0	2.604 ± 0.005
Dunaitsev (1973)	[28]	0	2.609 ± 0.008
Anderson (1960)	[29]	62 MeV/c	2.56 ± 0.8
Durbin (1952)	[30]	73 MeV/c	2.55 ± 0.19
Petrukhin (1969)	[31]	180 MeV/c	2.48 ± 0.04
Ayres (1971)	[32]	312 MeV/c	2.602 ± 0.004
Lobkowicz (1966)	[1]	1.6 and 2.0 GeV/c	2.667 ± 0.024

Table 2: Compilation of $\pi^{\pm}$ lifetime measurements.

Particle	E_{min} (GeV)	Ref	$\tau(E_{min})/\gamma$ (Secs)	E_{max} (GeV)	Ref	$\tau(E_{max})/\gamma$ (Secs)	Δ
$\mu^{\pm}$	0	[18]	$2.19703(4)\times10^{-6}$	3.1	[17]	$2.195(1)\times10^{-6}$	-0.00092(46)
$\tau^{\pm}$	2-5	[33]	$295(18)\times10^{-15}$	45	[18]	$295.6(3.1)\times10^{-15}$	0.00(6)
$\pi^{\pm}$	0	[18]	$2.603(4)\times10^{-8}$	1.8	[1]	$2.667(24)\times10^{-8}$	0.0246(90)
π^{0}	4-6	[34]	$8.2(4)\times10^{-17}$	235	[35]	$8.97(28)\times10^{-17}$	0.094(63)
$K^{\pm}$	0	[36]	$1.2380(16)\times10^{-8}$	3.0	[19]	$1.221(11)\times10^{-8}$	-0.0137(90)
K_S^0	2-5	[18]	$8.923(22)\times10^{-9}$	375	[5]	$8.83(60)\times10^{-9}$	-0.010(68)
Λ^0	≤ 1	[37]	$2.611(20)\times10^{-10}$	16.5	[20]	$2.7(2)\times10^{-10}$	0.03(7)
Ξ^0	≤ 1	[38]	$2.88(20)\times10^{-10}$	14	[20]	$2.78(4)\times10^{-10}$	-0.03(7)
Ξ^-	≤ 1	[38]	$1.63(3)\times10^{-10}$	131	[21]	$1.652(51)\times10^{-10}$	0.013(36)
Ω^-	≤ 1.7	[39]	$0.75(14)\times10^{-10}$	198	[22]	$0.811(37)\times10^{-10}$	0.08(16)

Table 3: Compilation of particle lifetime measurements at the lowest energies (E_{min}) and highest energies (E_{max}) appearing in the literature, and the corresponding fractional deviation Δ from the time dilation formula.

Particle	Limit on Δ (2σ)	Limit on α (2σ)
$\mu^{\pm}$	≤ 0.00092	$\leq 4.4 \times 10^{-16}$ cm
$\tau^{\pm}$	≤ 0.12	$\leq 3.4 \times 10^{-16}$ cm
$\pi^{\pm}$	≤ 0.0426	$\leq 5.1 \times 10^{-15}$ cm
π^{0}	≤ 0.22	$\leq 8.9 \times 10^{-17}$ cm
$K^{\pm}$	≤ 0.018	$\leq 2.0 \times 10^{-15}$ cm
K_S^0	≤ 0.136	$\leq 4.4 \times 10^{-17}$ cm
Λ^0	≤ 0.17	$\leq 1.1 \times 10^{-15}$ cm
Ξ^0	≤ 0.14	$\leq 1.2 \times 10^{-15}$ cm
Ξ^-	≤ 0.085	$\leq 9.6 \times 10^{-17}$ cm
Ω^-	≤ 0.11	$\leq 7.6 \times 10^{-17}$ cm

Table 4: Compilation of two standard deviation upper limits on the fundamental length α calculated from particle lifetime measurements listed in the preceeding table.

Measurement	Value	Ref.	δ	Limit (2σ)
$\tau_{\pi^\pm}$ ($\gamma = 13$)	$\Delta =$ 0.0246(90)	[1]	$-(1.1 \pm 0.4) \times 10^{-4}$	$\leq 8.0 \times 10^{-5}$
$\tau_{K^\pm}$ ($\gamma = 6.1$)	$\Delta =$ 0.0137(90)	[19]	$(4.3 \pm 2.8) \times 10^{-4}$	$\leq 9.9 \times 10^{-4}$
τ_{Λ^0} ($\gamma = 14.8$)	$\Delta =$ 0.03(7)	[20]	$(1.4 \pm 3.2) \times 10^{-4}$ for $c_2 = 1$	$\leq 7.8 \times 10^{-4}$
τ_{Ξ^0} ($\gamma = 10.6$)	$\Delta =$ -0.03(7)	[20]	$-(2.7 \pm 6.2) \times 10^{-4}$ for $c_2 = 1$	$\leq 1.2 \times 10^{-3}$
τ_{Ξ^-} ($\gamma = 99.1$)	$\Delta =$ 0.013(36)	[21]	$(1.3 \pm 3.7) \times 10^{-6}$ for $c_2 = 1$	$\leq 8.7 \times 10^{-6}$
τ_{Ω^-} ($\gamma = 118.$)	$\Delta =$ 0.08(16)	[22]	$(5.8 \pm 11.5) \times 10^{-6}$ for $c_2 = 1$	$\leq 2.9 \times 10^{-5}$
Michel parameter (ρ)	$\rho =$ 0.7518(26)	[18]	$-(0.0036 \pm 0.0052)$	≤ 0.010
$K_L - K_S$ mass difference		[16]		$\leq 8.7 \times 10^{-6}$
Eötvos experiments	$\Delta a/g =$ $-(3 \pm 9) \times 10^{-11}$	[16] [40]	$-(0.37 \pm 1.10) \times 10^{-3}$	$\leq 2.2 \times 10^{-3}$

Table 5: Compilation of two standard deviation upper limits on the fundamental Nielsen and Picek parameter δ which characterizes the size of the Lorentz non-invariant addition to the weak boson propagators.

L_2 (m)	a^2	b^2	N_1	N_2
20	1.57	0.063	2.3×10^6	2.0×10^5
30	2.05	0.18	3.2×10^6	5.0×10^5
40	2.77	0.44	4.5×10^6	1.2×10^6
50	4.01	1.00	6.8×10^6	2.4×10^6

Table 6: The number of $\pi^\pm$ decays that must be recorded N_1 and N_2 at decay lengths L_1 and L_2 to achieve a statistical precision of 0.1% on the measured lifetime. The numbers have been calculated to minimize the data taking time, and are shown as a function of the length L_2 for the choice $L_1 = 100$m. The parameters a and b are those shown in the expressions given in the text.

Beam Momentum (GeV/c)	Type	Particles per 5×10^{11} on target after collimation	Cherenkov phototube coincidence level	Cherenkov tagging efficiency	Tags per Spill	Tag rate (KHz)	Mistag fraction (%)
100	π^+	1.3×10^7	3-fold	0.47	6.1×10^6	306.	0.009
	π^-	1.4×10^7	3-fold	0.47	6.6×10^6	329.	0.008
	K^+	1.2×10^6	4-fold	0.079	9.5×10^4	4.74	0.44
	K^+	1.2×10^6	5-fold	0.017	2.0×10^4	1.02	0.037
	K^-	1.2×10^6	4-fold	0.079	9.5×10^4	4.74	0.43
	K^-	1.2×10^6	5-fold	0.017	2.0×10^4	1.02	0.037
400	π^+	6.7×10^6	3-fold	0.54	3.6×10^6	181.	0.025
	π^-	1.1×10^7	3-fold	0.54	5.9×10^6	297.	0.007
	K^+	1.3×10^6	4-fold	0.42	5.5×10^5	27.3	0.12
	K^+	1.3×10^6	5-fold	0.14	1.8×10^5	9.10	0.006
	K^-	4.4×10^5	4-fold	0.42	1.8×10^5	9.24	0.16
	K^-	4.4×10^5	5-fold	0.14	6.2×10^4	3.08	0.008
530	π^+	1.3×10^6	4-fold	0.24	3.1×10^5	15.6	0.006
	π^-	3.6×10^6	3-fold	0.53	1.9×10^6	95.4	0.010
	K^+	4.4×10^5	4-fold	0.30	1.3×10^5	6.60	0.86
	K^+	4.4×10^5	5-fold	0.11	4.8×10^4	2.42	0.043
	K^-	7.1×10^4	4-fold	0.30	2.1×10^4	1.07	0.46
	K^-	7.1×10^4	5-fold	0.11	7.8×10^3	0.39	0.022
600	π^+	4.3×10^5	4-fold	0.24	1.0×10^5	5.16	0.018
	π^-	1.4×10^6	3-fold	0.54	7.6×10^5	37.8	0.013
	K^+	1.7×10^5	6-fold	0.018	3.1×10^3	0.15	0.004
	K^-	1.6×10^4	6-fold	0.018	2.9×10^2	0.014	0.002

Table 7: Summary of Cherenkov tagging rates and mistag fractions when there are 5×10^{11} protons on the primary target per 20 second spill. The tagging rates, which were calculated with the Cherenkov Monte Carlo program described in the text, correspond to the secondary particle fluxes shown in Fig. 7.

Item	Number of Channels	Data Size (bytes)
Cherenkov Counter		
PMT's	18	72
Scintillator Counters		
Veto counters (PMT's)	28	112
Trigger counters (PMT's)	7	28
Tracking Stations		
T1+T2 Proportional tubes	128	64
T3+T4 Proportional tubes	512	128
Electromagnetic Calorimeter		
PMT's	4	16
Hadronic Calorimeter		
Channels	56	224
Muon Identifier		
PMT's	12	48
Proportional Tubes	96	24
TOTAL	861	716

Table 8: Total number of electronic channels and their estimated contributions to the event record size. Each channel is read out with both an ADC and a TDC. We assume that we will use zero suppression for all proportional tubes.

Beam Momentum (GeV/c)	Type	Cherenkov phototube coincidence level	Tag rate (KHz)	Geometrical acceptance (%)	Decay fraction per 100m (%)	$\mu\nu$ Decay trigger rate (Hz)	Triggers per spill
	π^+	3-fold	306		1.8	936	18727
	π^-	3-fold	329		1.8	1007	20135
100	K^+	4-fold	4.74	17	13.1	67.0	1341
	K^+	5-fold	1.02		13.1	14.4	289
	K^-	4-fold	4.74		13.1	67.0	1341
	K^-	5-fold	1.02		13.1	14.4	289
	π^+	3-fold	181		0.45	138	2769
	π^-	3-fold	297		0.45	227	4544
400	K^+	4-fold	27.3	17	3.29	97.0	1939
	K^+	5-fold	9.10		3.29	32.3	646
	K^-	4-fold	9.24		3.29	32.8	656
	K^-	5-fold	3.08		3.29	10.9	219
	π^+	4-fold	15.6		0.34	9.0	180
	π^-	3-fold	95.4		0.34	55.1	1103
530	K^+	4-fold	6.60	17	2.48	17.7	353
	K^+	5-fold	2.42		2.48	6.5	130
	K^-	4-fold	1.07		2.48	2.9	57.3
	K^-	5-fold	0.39		2.48	1.0	20.9
	π^+	4-fold	5.16		0.30	2.6	52.6
600	π^-	3-fold	37.8	17	0.30	19.3	386
	K^+	6-fold	0.15		2.19	0.35	7.09
	K^-	6-fold	0.014		2.19	0.033	0.66

Table 9: Summary of calculated trigger rates for a decay length of 100m. The kaon $\mu\nu$ trigger rates include the branching fraction $\mathrm{BR}(K^\pm \to \mu^\pm\nu) = (63.51 \pm 0.18)\%$.

Energy	Data sample	Beam time at 100m	Beam time at 50m	Beam time at 30m
100 GeV	π^+ decays	71 hours	30 hours	15 hours
	π^- decays	71 hours	30 hours	15 hours
	muon beam	48 hours	48 hours	48 hours
530 GeV	π^+ decays	1267 hours	897 hours	452 hours
	π^- decays	214 hours	153 hours	81 hours
	muon beam	48 hours	48 hours	48 hours
800 GeV	10^6 protons	15 hours	15 hours	15 hours
	TOTAL	1734 hours	1221 hours	674 hours

Table 10: Summary of beam time requirements to make precision measurements of the π^+ and π^- lifetimes at 100 GeV and 530 GeV. The tabulated beam times would enable us to record 6.8×10^6 decays at 100m, 2.4×10^6 decays at 50m, and 8×10^5 decays at 30m. The estimates include a factor of 50% for the accelerator efficiency and 8 hours per measurement setup time. It is also assumed that the maximum rate at which decays can be recorded is 180 Hz.

Item	Cost (K$)	Subtotals (K$)
Beam Enclosure MW8		
Relocate upstream of Cherenkov:		
MW8CC, MW8CV, MW8CH, MW8IC		
Rigging	4.0	
Electrical/Controls	2.0	
Subtotal		6.0
Remove to MW9 hall:		
MW8Q4-1/2, MW8D, MW8Q5-1/2, MW8Q6		
MW8V2-1/2, MW8H, MW8Q7-1/2, MW8Q8		
Rigging	5.0	
Install:		
EPB1/2	2.0	
Vacuum system for EPB1/2	0.3	
LC water for EPB1/2	0.3	
2 x (4 x MCM500) for EPB1/2	0.5	
Subtotal		8.1
Experimental Hall MW9		
Build platforms (concrete blocks)		
100m decay ($8 \times 6' \times 3' \times 3'$) blocks	4.0	
50m decay ($4 \times 6' \times 3' \times 3'$) blocks	2.0	
Install:		
EPB3/4	2.0	
Vacuum system for EPB3/4	0.3	
LC water for EPB3/4	1.5	
2 x (4 x MCM500) for EPB3/4	7.2	
Vacuum decay pipe	1.0	
Vacuum system for decay pipe	0.3	
Subtotal		18.3
TOTAL		32.4

Table 11: Summary of beamline and experimental hall costs.

Item	Fermilab Costs (K$)	Other Costs (K$)	Proposed Institution
Decay Pipe and Stands			
Decay pipe fabrication	1.0		FNAL/RD
Vacuum windows ×6	2.0		FNAL/RD
Stands EPB's and Decay pipe	6.3		FNAL/RD
Scintillator Counters			
PMT's (recycled)			
Veto counters	5.6		FNAL/PS
Trigger counters	1.4		FNAL/PS
Stands ×7	2.1		FNAL/RD
Tracking Stations T1/T2/T3/T4			
Chamber construction and support frame		20.0	Duke
Amplifier and discriminator cards		6.0	Duke
Electromagnetic Calorimeter (existing)			
PMT's (recycled)			
Stand	1.5		FNAL/RD
Hadronic Calorimeter (existing)			
Additional Modules x 2		8.0	Rockefeller
Stand	3.0		FNAL/RD
Muon Identifier			
Steel machining		3.0	Nebraska
Scintillation counters x 12	2.4		FNAL/PS
PMT's (recycled)			
Proportional tubes		4.0	Nebraska
Stand	3.0		FNAL/RD
Cables			
RG58, RG8 Foam, HV	36.0		FNAL/PS
Twisted pairs	15.0		FNAL/PS
Total Equipment	79.3	41.0	

Table 12: Summary of detector costs.

Item	Fermilab Costs (K$)	Other Costs (K$)	Institution
Tracker Electronics			
4291B TDCs (20)		13.0	Duke
4298 Controller (1)		4.5	Duke
4299 Camac interface (1)		3.0	Duke
2 x "Droege" HV Power Supplies			FNAL/CD
Hadron Calorimeter			
4 ADC type LeCroy 2249A units			FNAL/CD
2 "Droege" HV supplies			FNAL/CD
Muon Identifier			
Frontend		2.0	Nebraska
4291B TDCs (4)			FNAL/CD
1 x "Droege" HV Power Supply			FNAL/CD
Trigger Logic, PMT'S			FNAL/CD
20 x Octal Discriminators			FNAL/CD
4 x Dual LC 364 coincidence units			FNAL/CD
3 x Majority coincidence unit			FNAL/CD
10 x Dual LC 365 coincidence units			FNAL/CD
50 Channels Camac Scalers			FNAL/CD
4 x Dual Visual Scalers			FNAL/CD
1 x Visual scaler with preset			FNAL/CD
90 ADC channels			FNAL/CD
90 TDC channels			FNAL/CD
HV Supplies (Total 4KV x 180 mA)			FNAL/CD
HV Distribution for 90 channels			FNAL/CD
6 x CAMAC crate controllers			FNAL/CD
6 x High Power NIM Bins			FNAL/CD
6 x High Power CAMAC crates			FNAL/CD
Subtotal new equipment only	10.0	22.5	
DAQ			
Unix Workstation			FNAL/CD
SCSI Jorway Interface			FNAL/CD
Gigabyte tapedrive x 2			FNAL/CD
X-Terminals x 4			FNAL/CD
Postscript laser printer			FNAL/CD
Subtotal DAQ new equipment only	20.0		
Total new equipment only	30.0	22.5	

Table 13: Electronics and DAQ equipment request. Note that we expect most of the Fermilab PREP/DAQ equipment come from existing equipment, but allow $10K/$20K for new items.

Item	Fermilab Costs (K$)	Other Costs (K$)	Proposed Institution
Fermilab Costs			
MW8 and MW9 Costs (Table 11)	32.4		FNAL/RD
Detector systems (Table 12)	18.9		FNAL/RD
	60.4		FNAL/PS
PREP new equipment (Table 13)	10.0		FNAL/CD
DAQ new equipment (Table 13)	20.0		FNAL/CD
Duke Costs			
Detector systems (Table 12)		26.0	Duke
Electronics (Table 13)		20.5	Duke
Nebraska Costs			
Detector systems (Table 12)		7.0	Nebraska
Electronics (Table 13)		2.0	Nebraska
Rockefeller Costs			
Detector systems (Table 12)		8.0	Rockefeller
Total Equipment	141.7	63.5	
Other Support			
Alignment	8 crew/days		FNAL/RD
Magnet Measurements	4 person/days		FNAL/TSS

Table 14: Overall summary of costs.

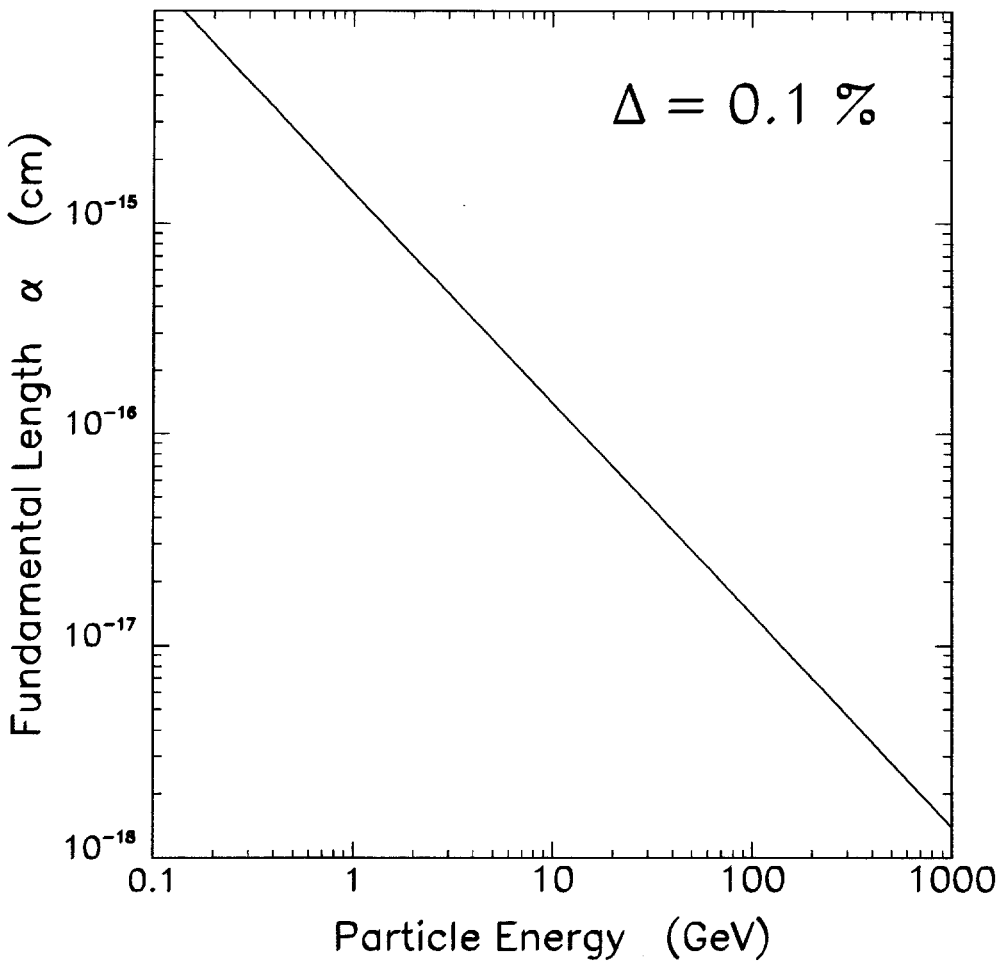

Figure 1: As a function of particle energy, the fundamental length α that will result in a deviation of 0.1% from the time dilation formula prediction for the lifetime of a particle. Note that α is the length below which microcausality is violated.

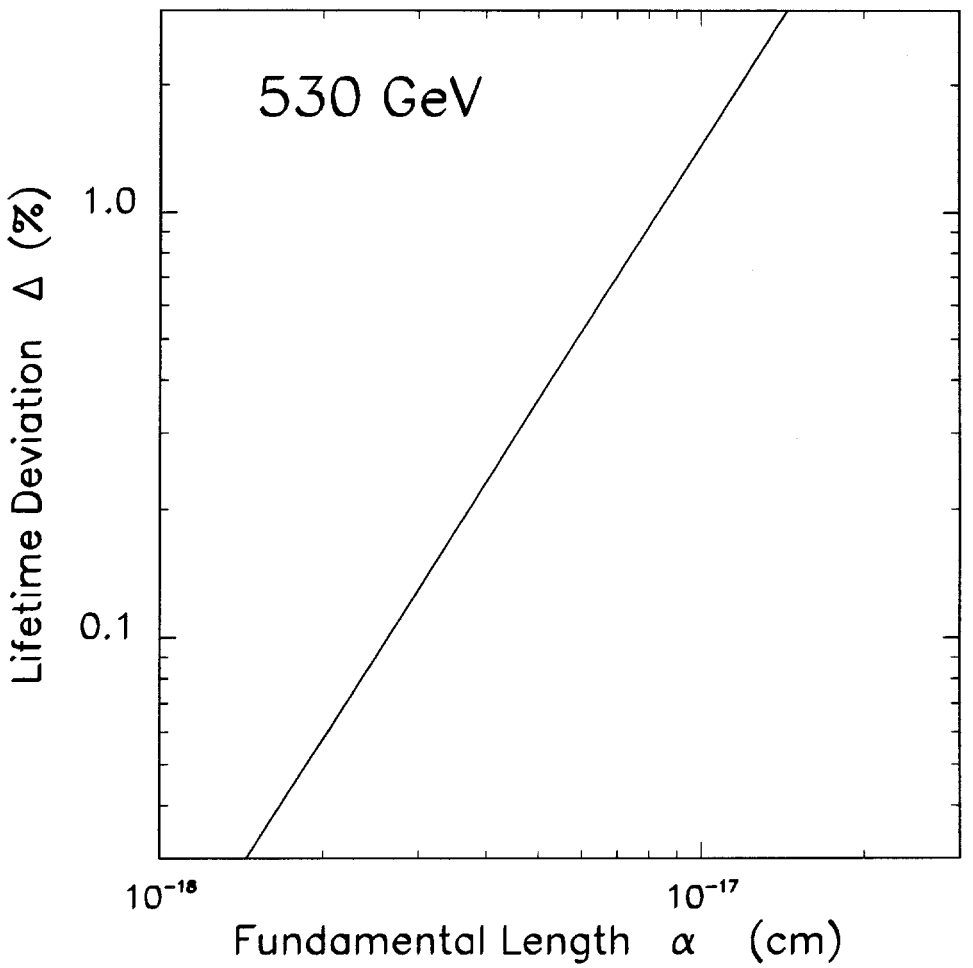

Figure 2: Deviation of the predicted lifetime of a particle with an energy of 530 GeV from the value given by the time dilation formula, shown as a function of the fundamental length α below which microcausality is violated.

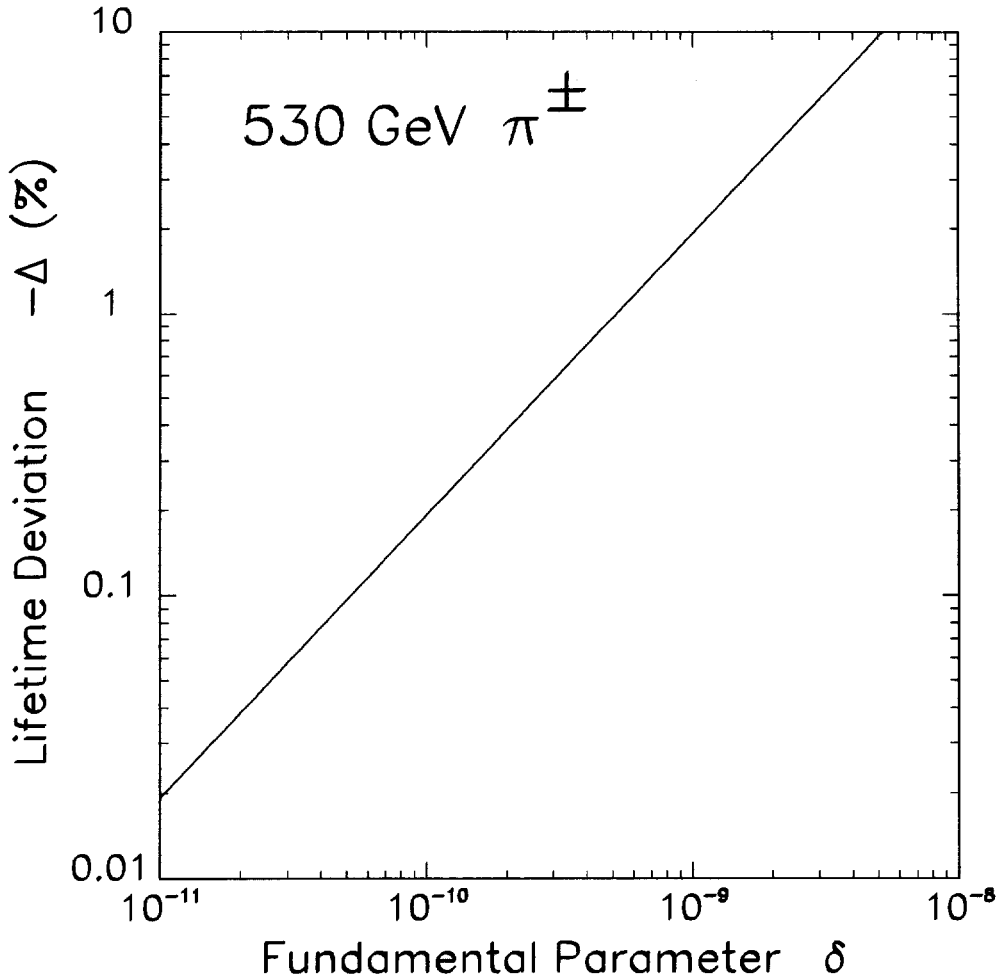

Figure 3: Deviation of the predicted lifetime of a particle with an energy of 530 GeV from the value given by the time dilation formula, shown as a function of the fundamental Nielsen and Picek parameter δ which describes the size of the Lorentz non-invariant contribution to the metric in the weak interaction Hamiltonian.

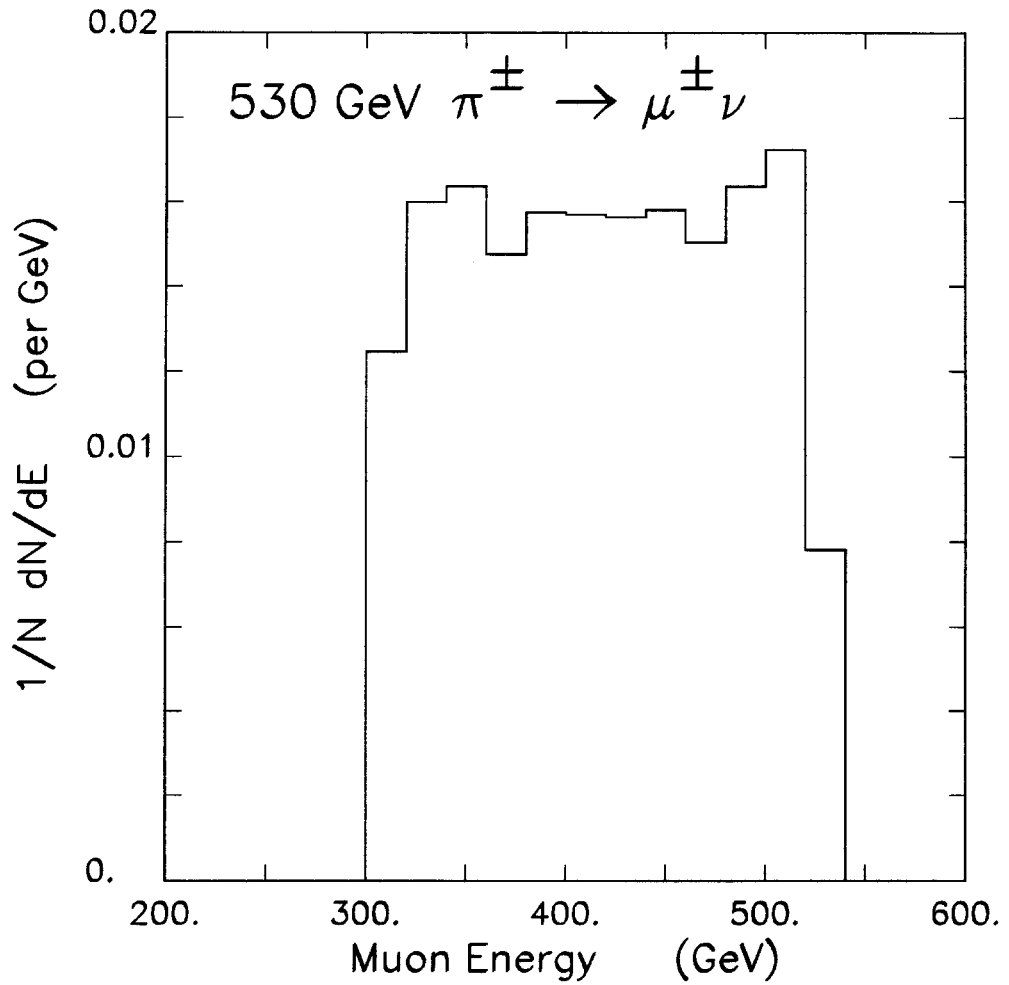

Figure 4: Distribution of muon energies calculated for the decays of 530 GeV pions.

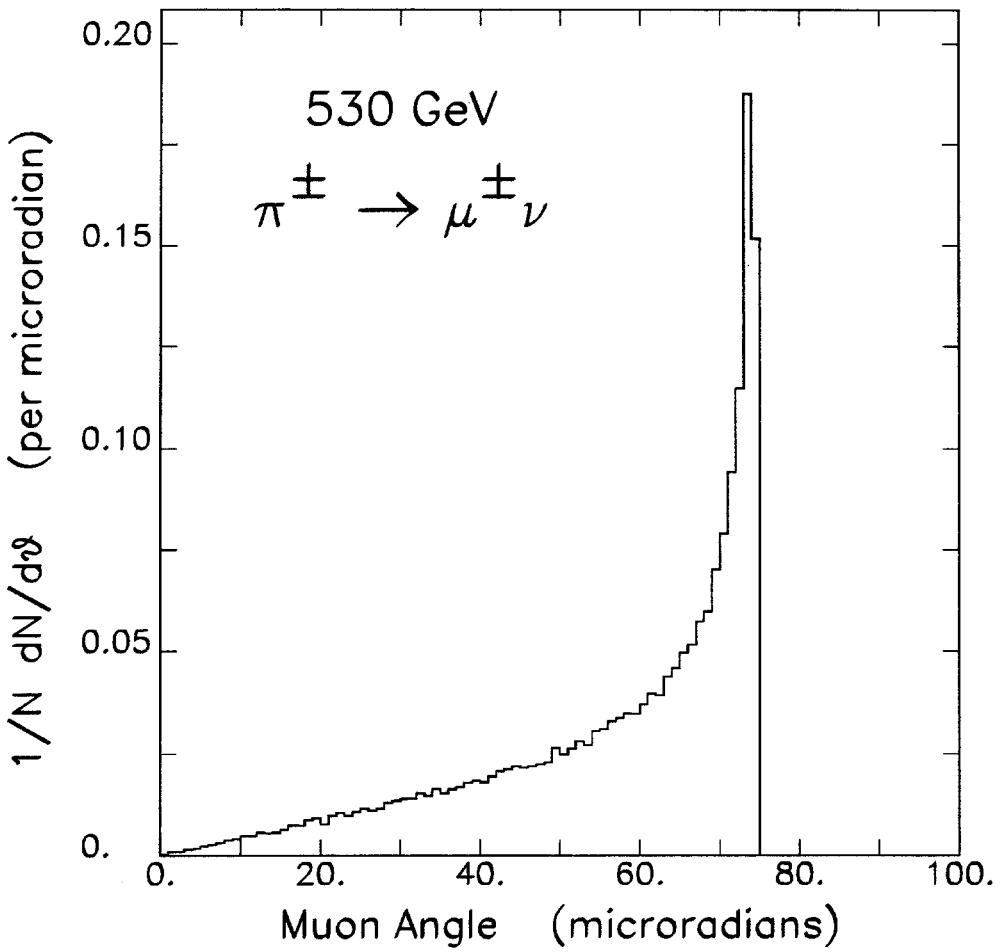

Figure 5: Distribution of angles between the parent pion flight direction and the decay muon direction, calculated for the decays of 530 GeV pions.

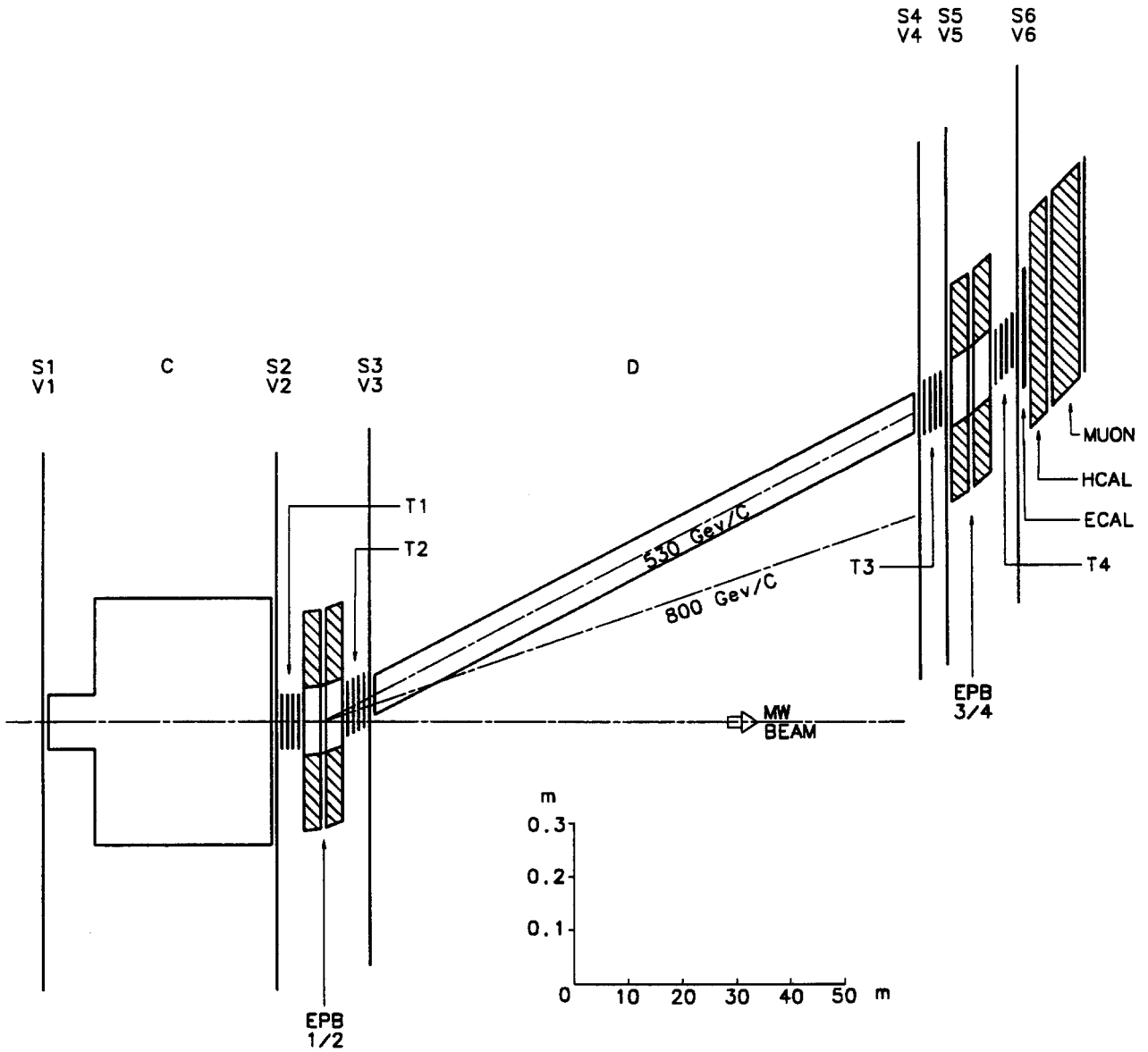

Figure 6: Schematic of the detector. The differential Cherenkov counter C is already installed in the MW beamline. The scintillators S1, S2, S3, and S4 together with the magnets EPB-1 and EPB-2 and the trackers T1 and T2 form the upstream momentum selector and spectrometer. The trackers T3 and T4 together with the magnets EPB-3 and EPB-4 form the downstream momentum analyzer. ECAL and HCAL are electromagnetic and hadronic calorimeters and MUON is a muon tagger. The veto counter systems V1 - V6 reject beam halo and nuclear interactions.

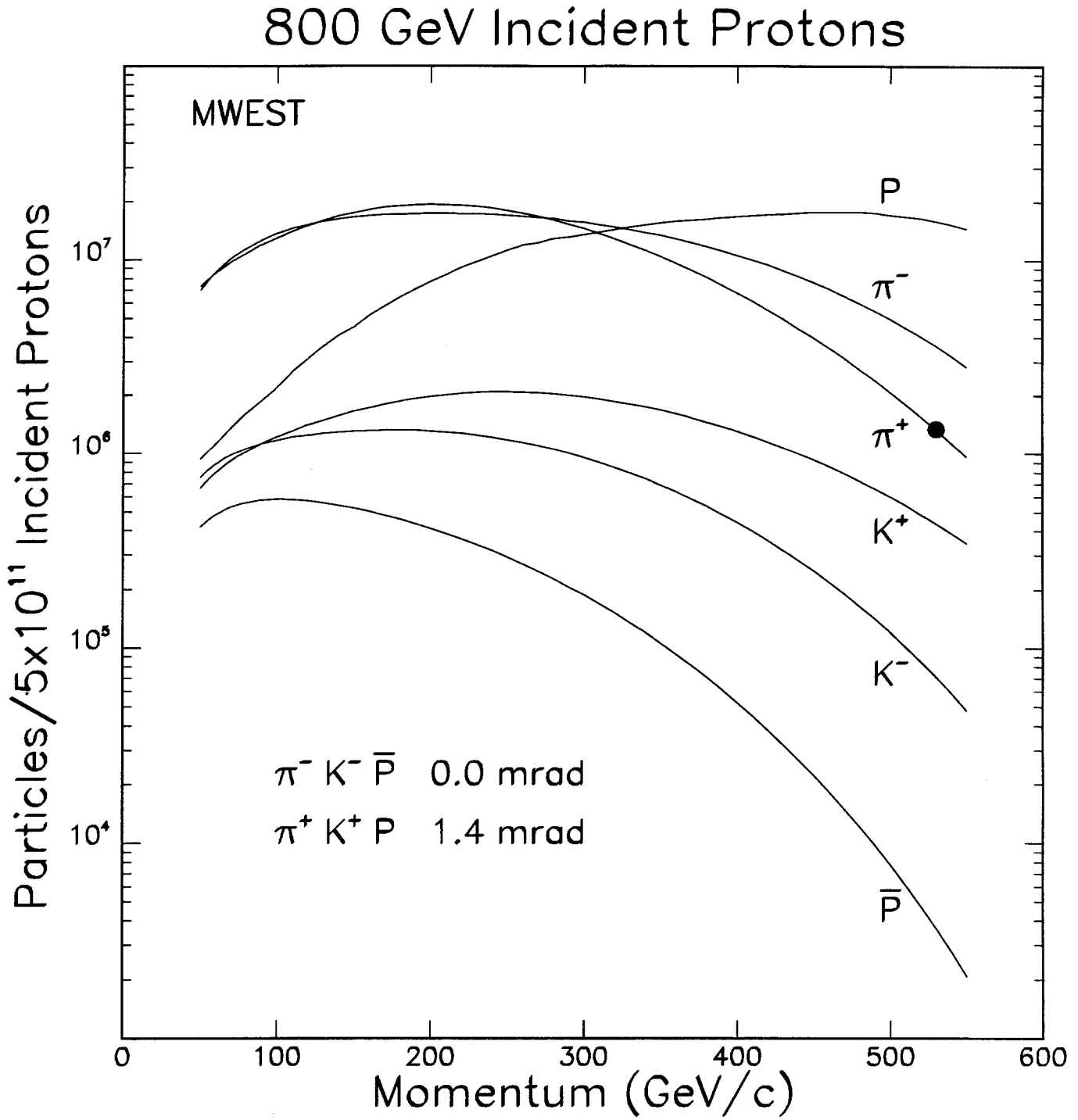

Figure 7: Secondary particle fluxes in the MW beamline when there are 5×10^{11} protons per spill incident on a 0.75 interaction length Beryllium target. The curves show the predictions of the Malensek particle production model (FN-341) normalized to the π^+ point at 530 GeV/c which was measured with collimators closed to obtain a beam momentum spread $\Delta P/P = 0.03$.

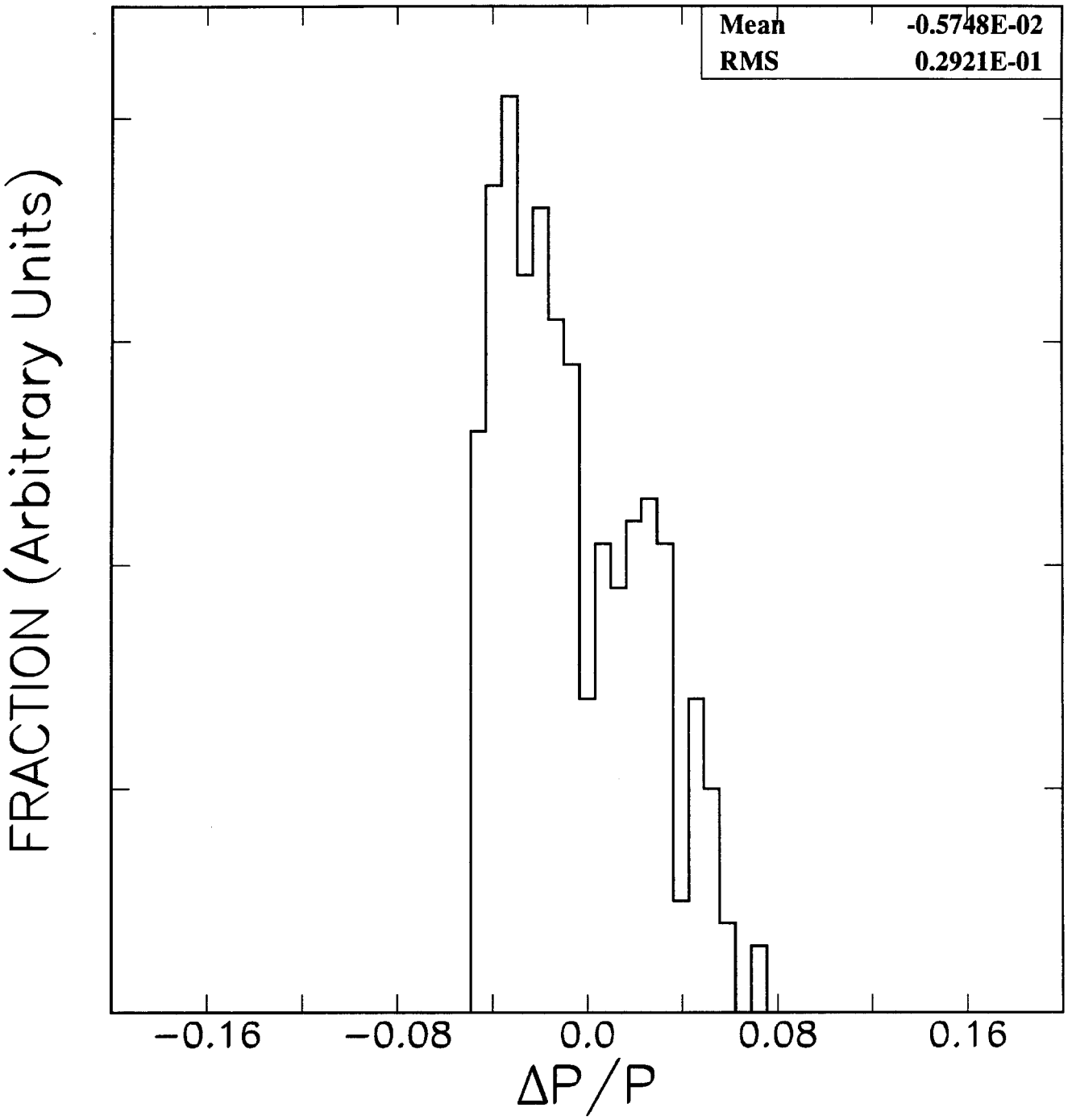

Figure 8: TURTLE Monte Carlo prediction for the beam momentum distribution at the Cherenkov counter with the collimators closed to select a narrow momentum bite.

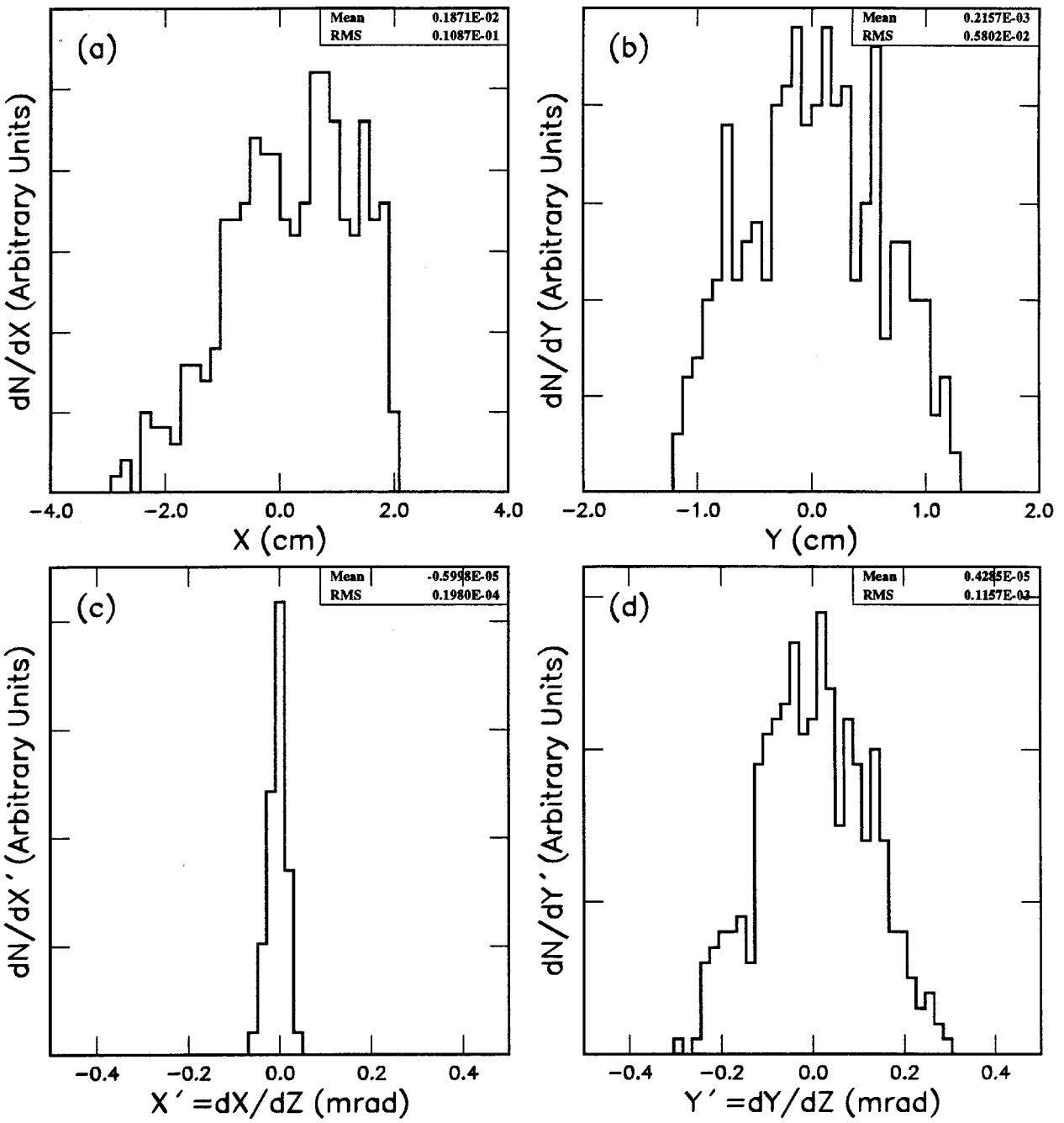

Figure 9: Predicted beam characteristics at the Cherenkov counter. The predictions were obtained using TURTLE Monte Carlo simulation.

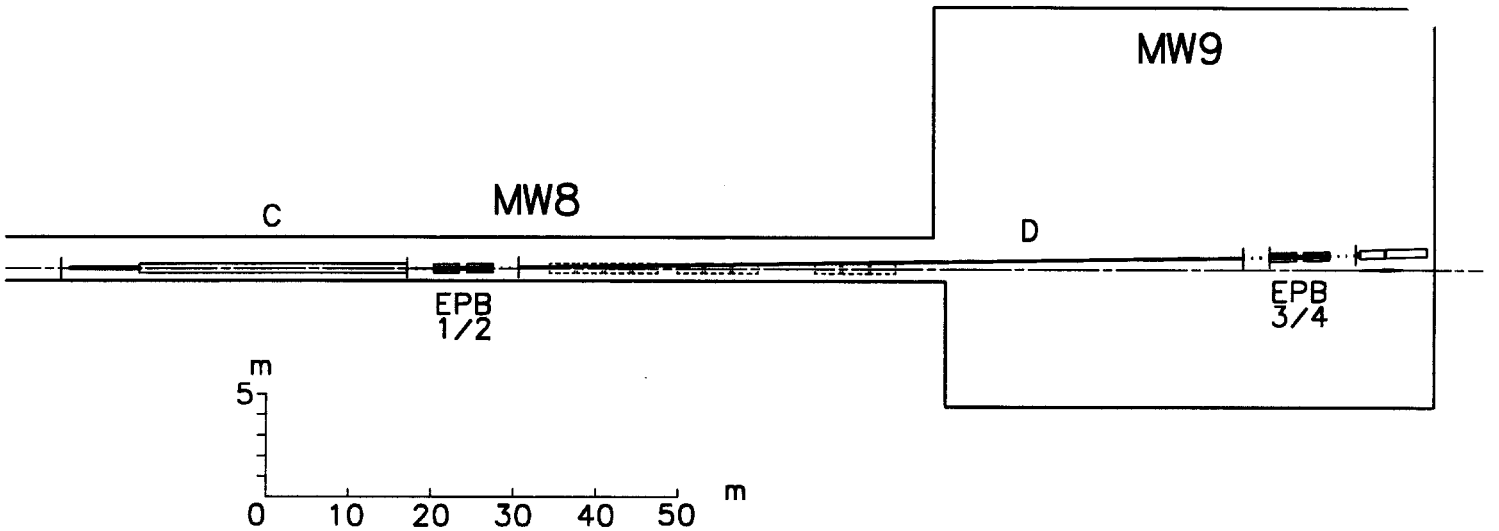

Figure 10: Location of the experiment in the MWEST beamline and experimental hall.

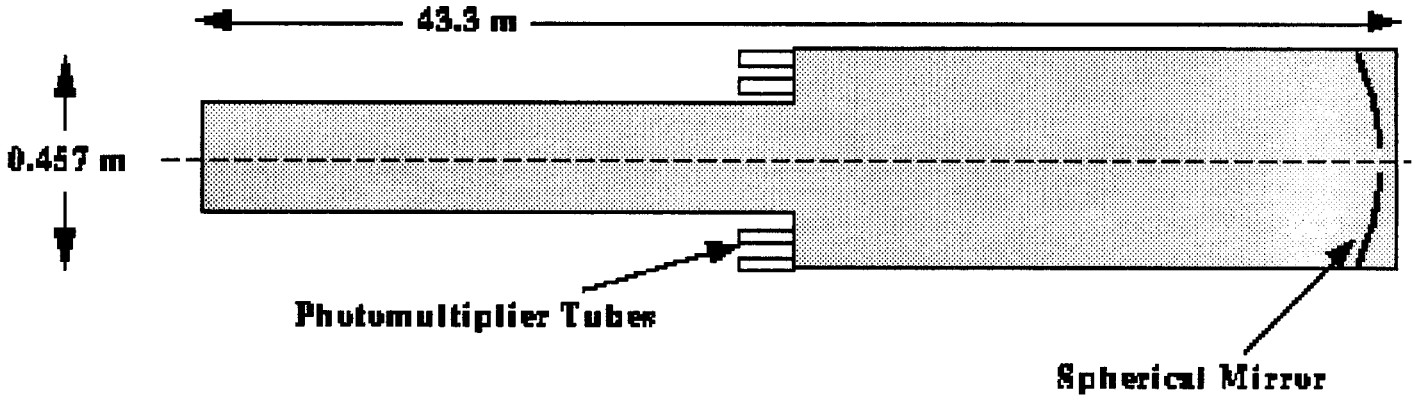

Figure 11: Schematic of the differential Cherenkov counter in the MW beamline.

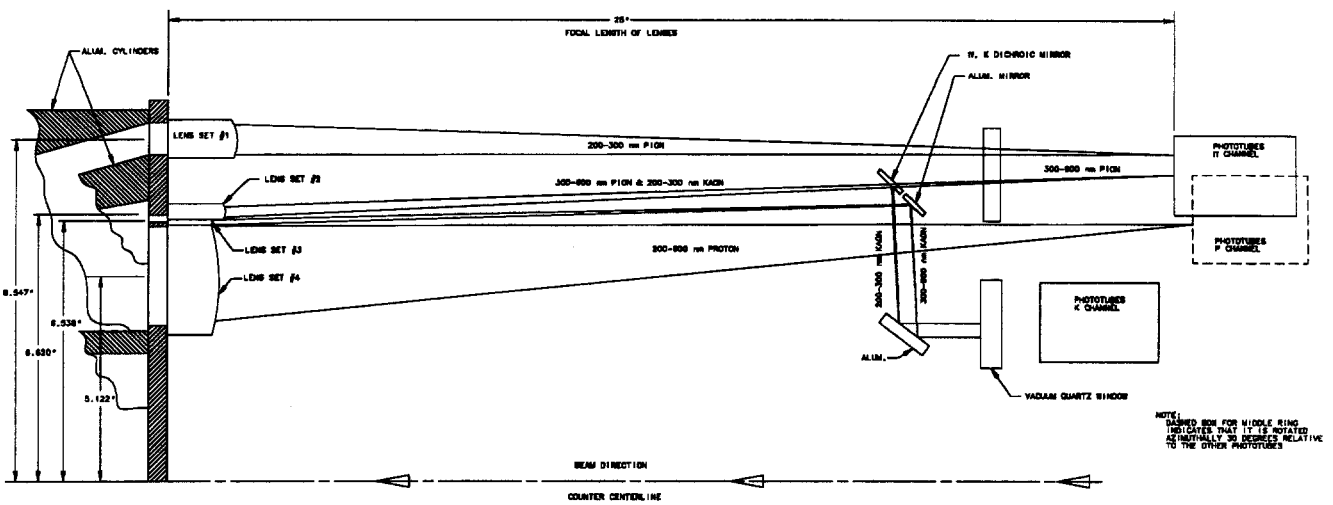

MWEST CERENKOV COUNTER OPTICS

Figure 12: Schematic of the differential Cherenkov counter optics.

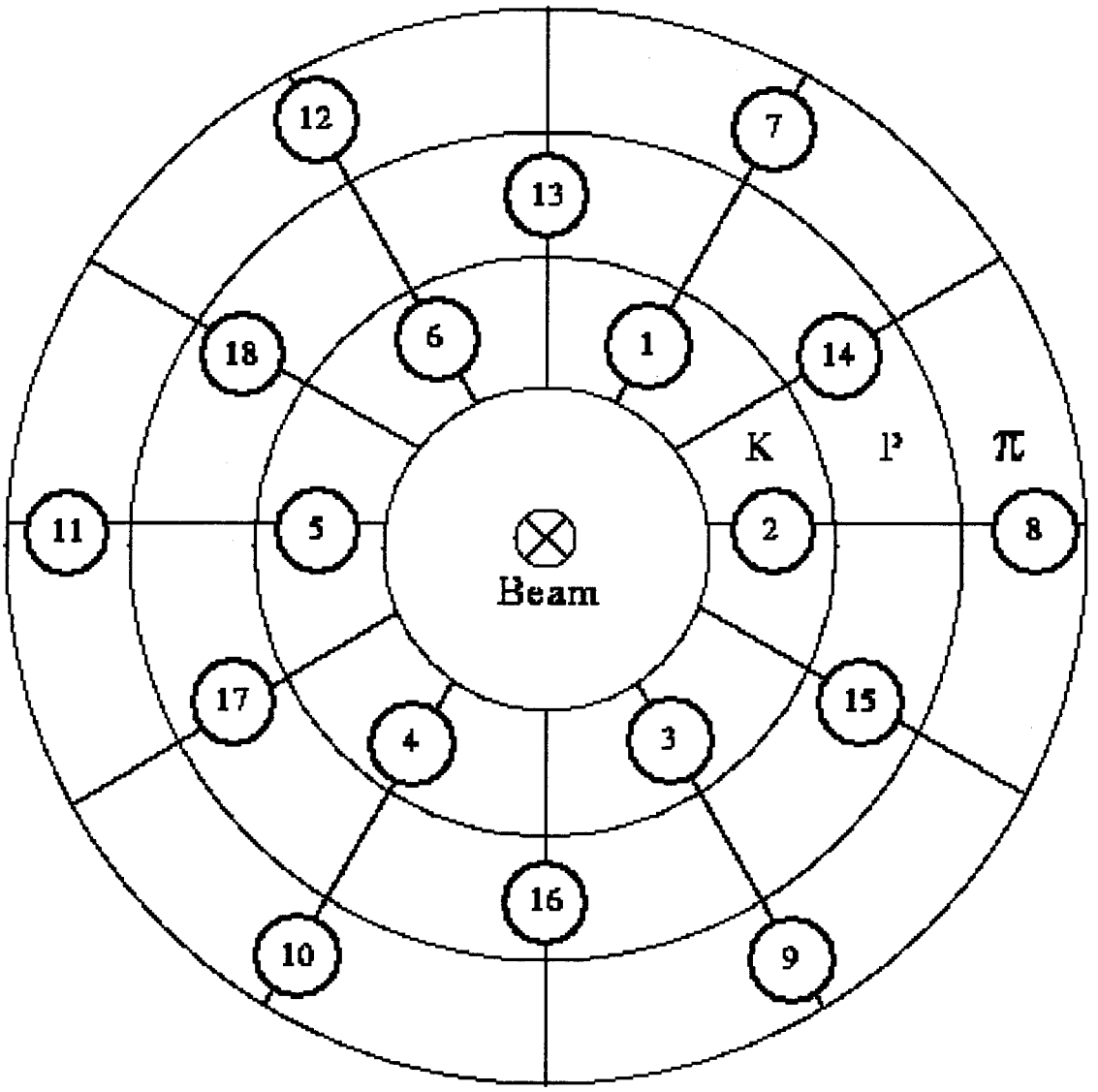

Figure 13: Schematic of the phototube arrangement at the upstream end of the differential Cherenkov counter.

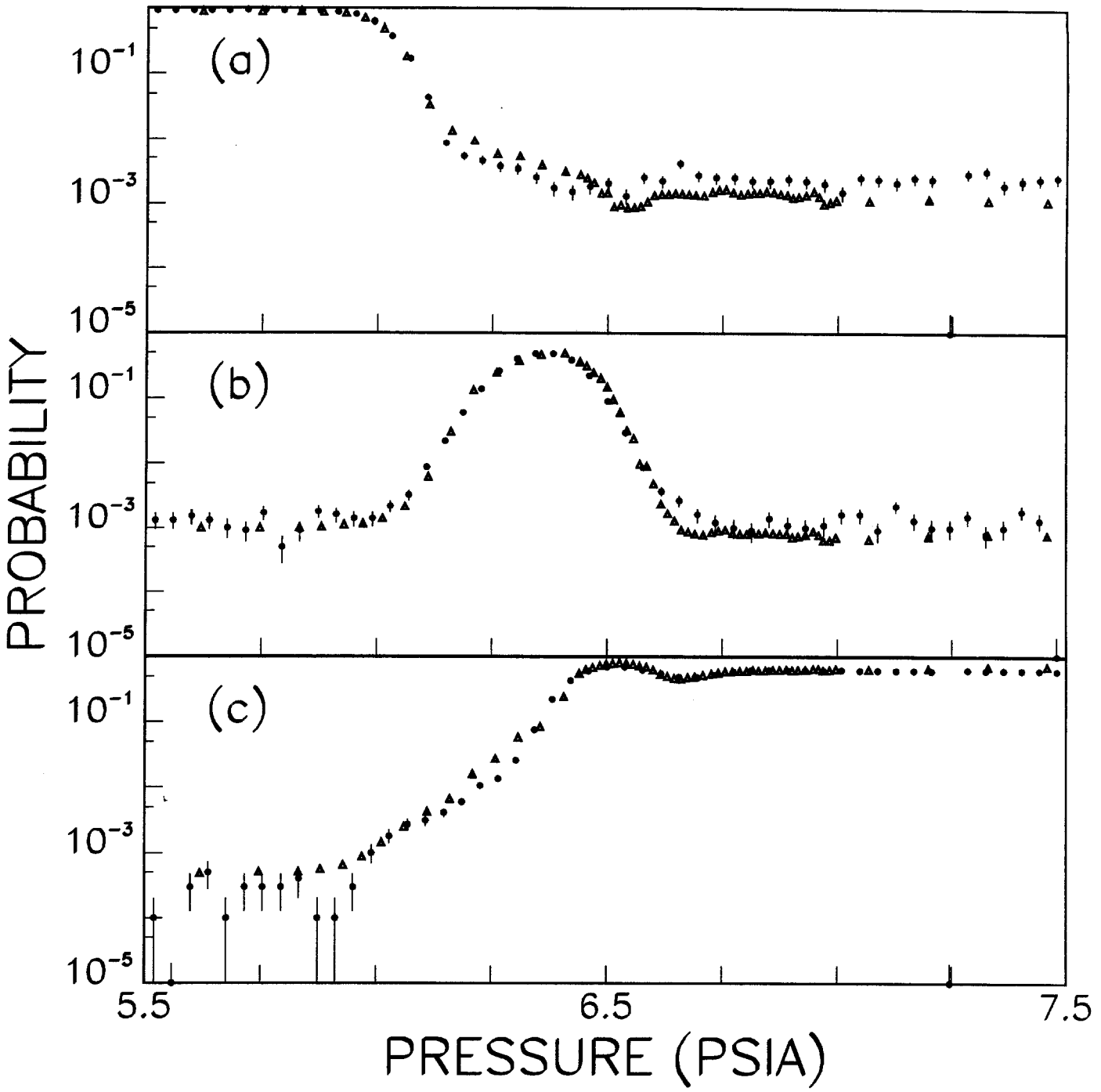

Figure 14: Response of the differential Cherenkov counter to 800 GeV protons (triangles) compared with Monte Carlo predictions (points). The Cherenkov efficiencies are shown as a function of Helium pressure for (a) the p-channel when there are at least two p-channel phototubes above threshold, (b) the K-channel when there are at least three K-channel phototubes above threshold, and (c) the π-channel when there are at least two π-channel phototubes above threshold and not more than one p-channel phototube above threshold.

π^- Tag Efficiencies and Backgrounds

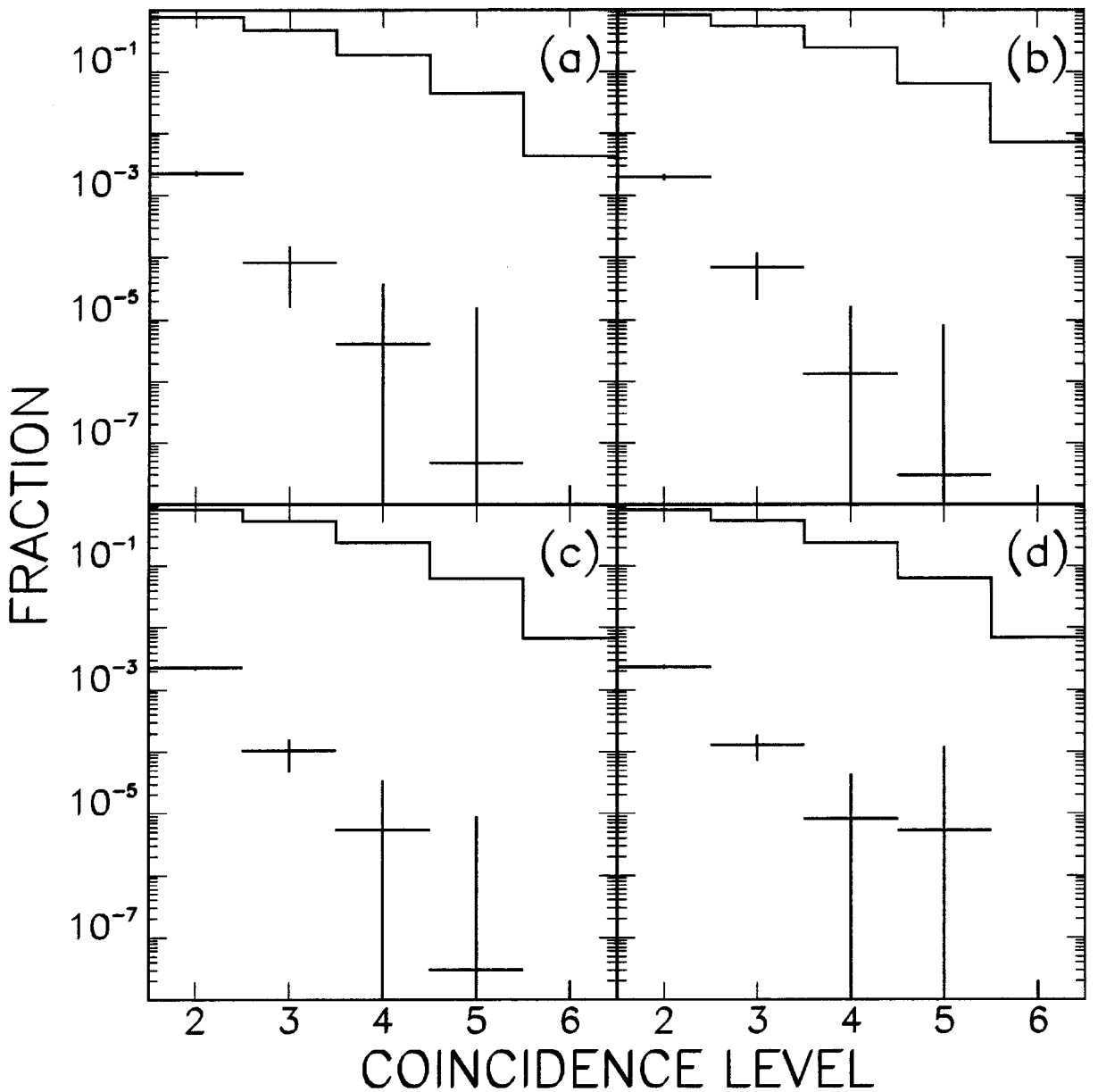

Figure 15: Predicted Cherenkov π^- tagging efficiencies (histograms) and mistag fractions (points) shown as a function of the minimum number of π-channel phototubes required to be above threshold. The four sets of plots show predictions for (a) 100 GeV/c, (b) 400 GeV/c, (c) 530 GeV/c, and (d) 600 GeV/c beams respectively.

π^+ Tag Efficiencies and Backgrounds

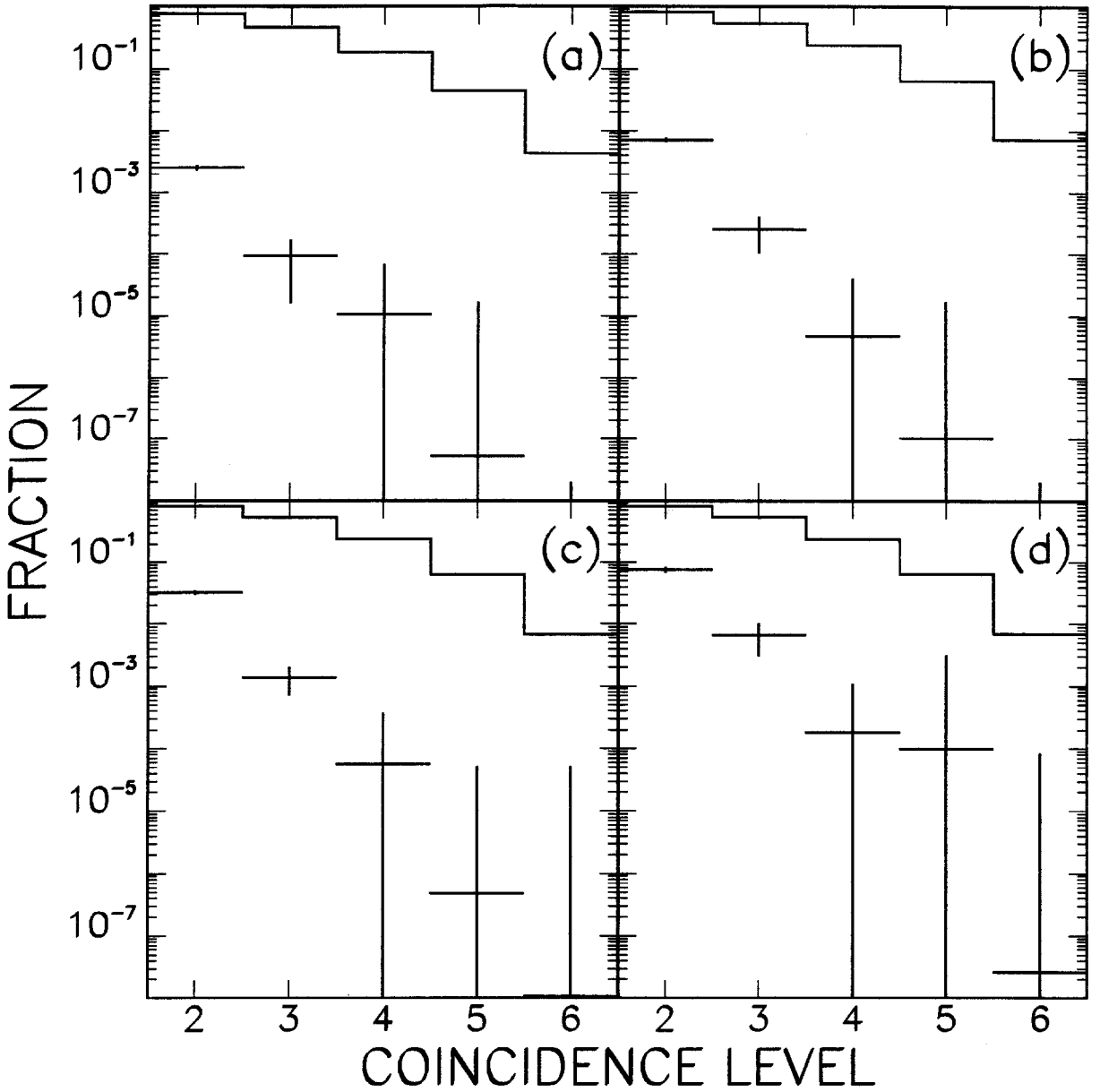

Figure 16: Predicted Cherenkov π^+ tagging efficiencies (histograms) and mistag fractions (points) shown as a function of the minimum number of π-channel phototubes required to be above threshold. The four sets of plots show predictions for (a) 100 GeV/c, (b) 400 GeV/c, (c) 530 GeV/c, and (d) 600 GeV/c beams respectively.

K^- Tag Efficiencies and Backgrounds

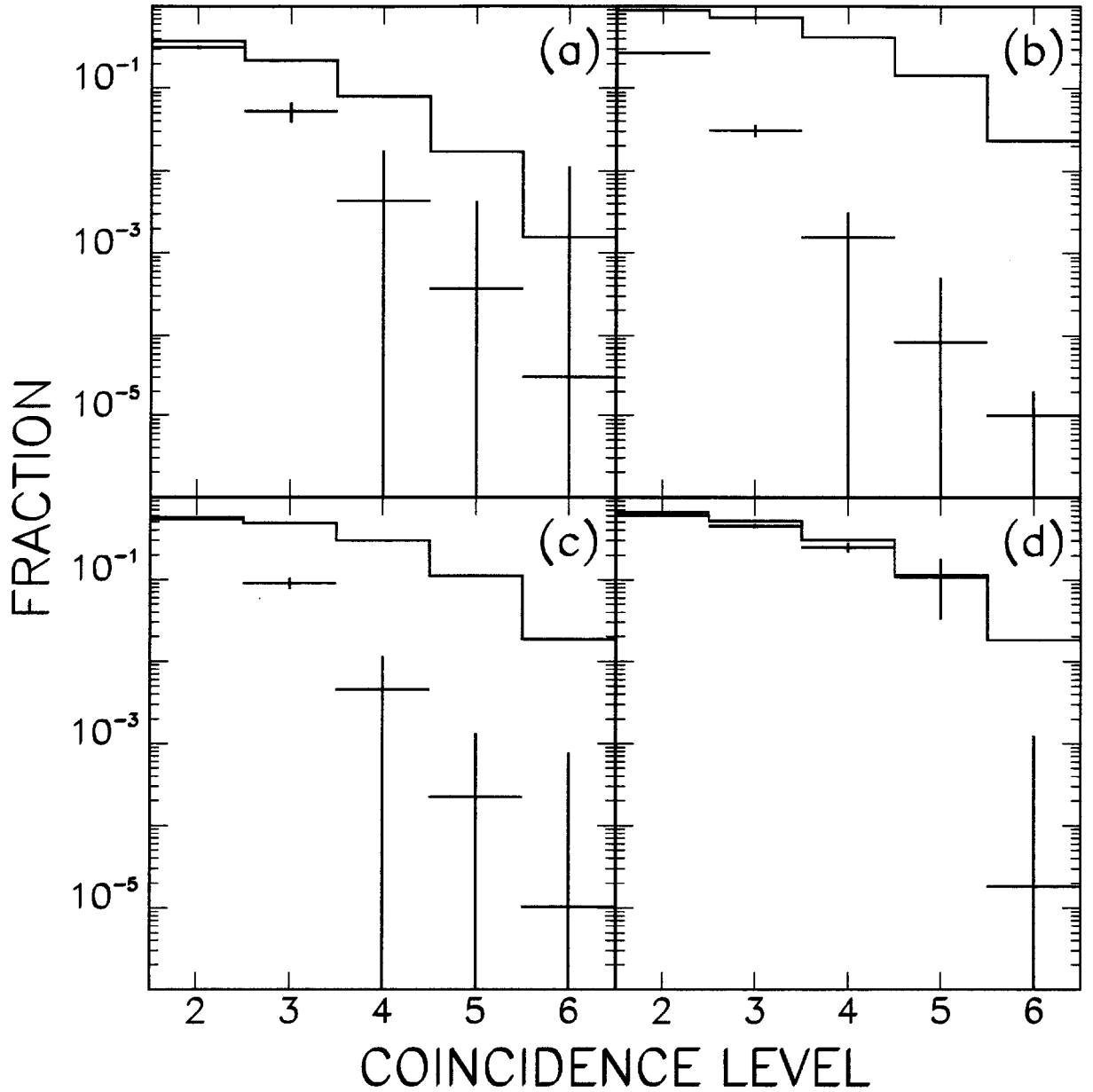

Figure 17: Predicted Cherenkov K^- tagging efficiencies (histograms) and mistag fractions (points) shown as a function of the minimum number of K-channel phototubes required to be above threshold. The four sets of plots show predictions for (a) 100 GeV/c, (b) 400 GeV/c, (c) 530 GeV/c, and (d) 600 GeV/c beams respectively.

K^+ Tag Efficiencies and Backgrounds

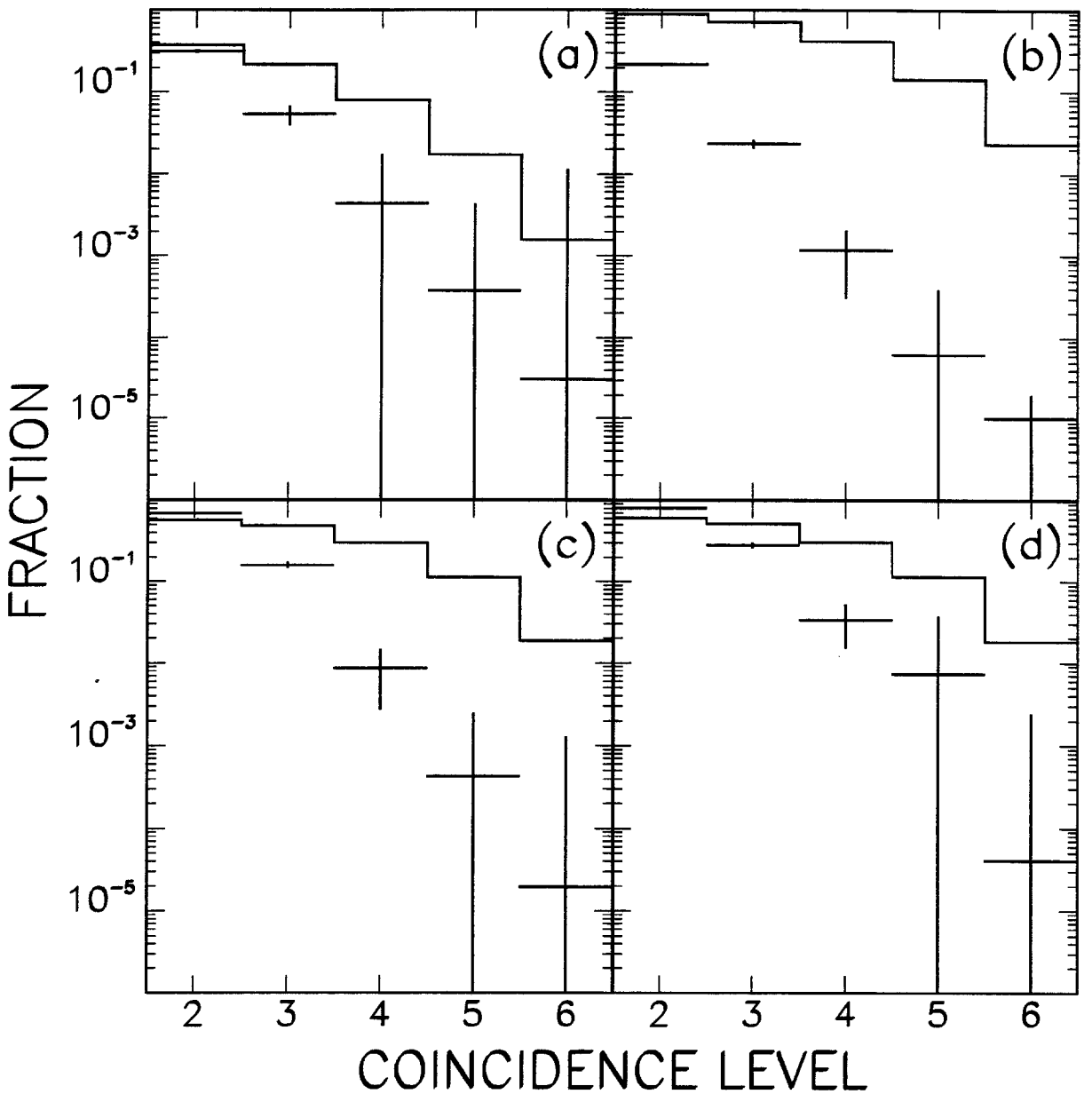

Figure 18: Predicted Cherenkov K^+ tagging efficiencies (histograms) and mistag fractions (points) shown as a function of the minimum number of K-channel phototubes required to be above threshold. The four sets of plots show predictions for (a) 100 GeV/c, (b) 400 GeV/c, (c) 530 GeV/c, and (d) 600 GeV/c beams respectively.

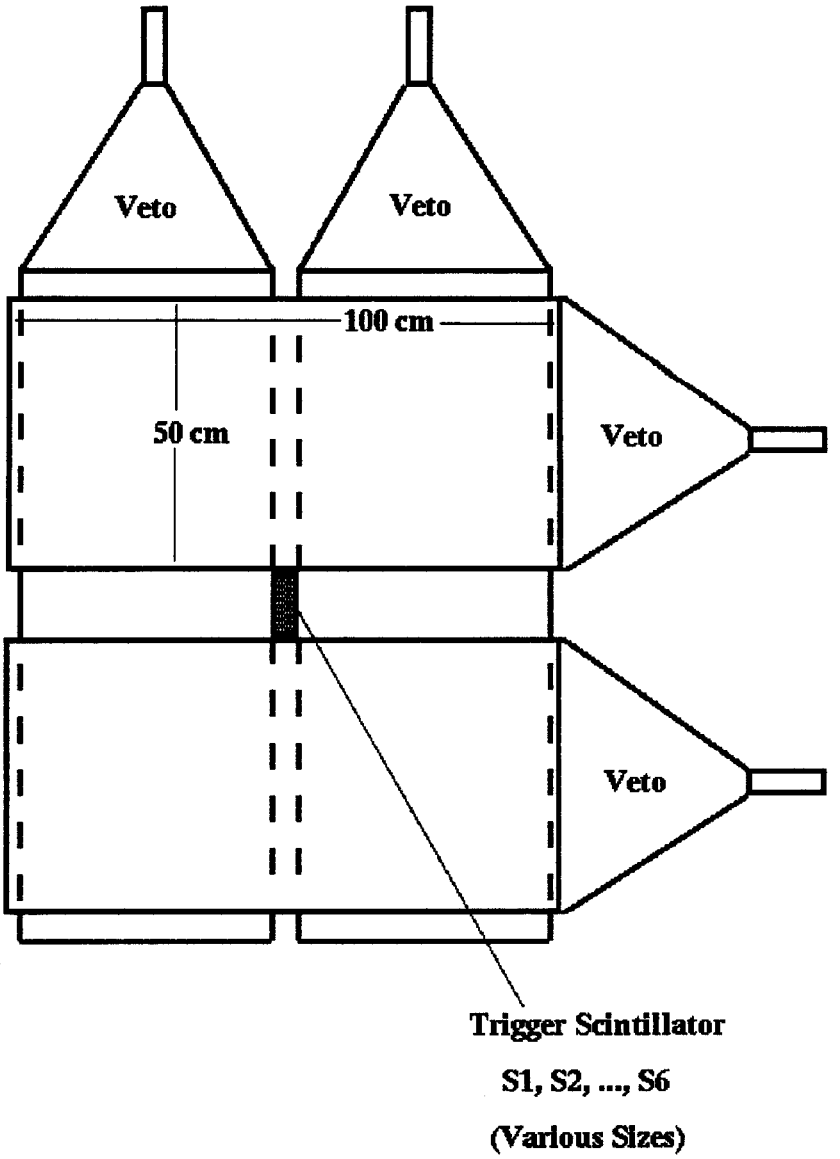

Figure 19: Schematic of the arrangement of veto counters (V) about each of the triggering counters (S).

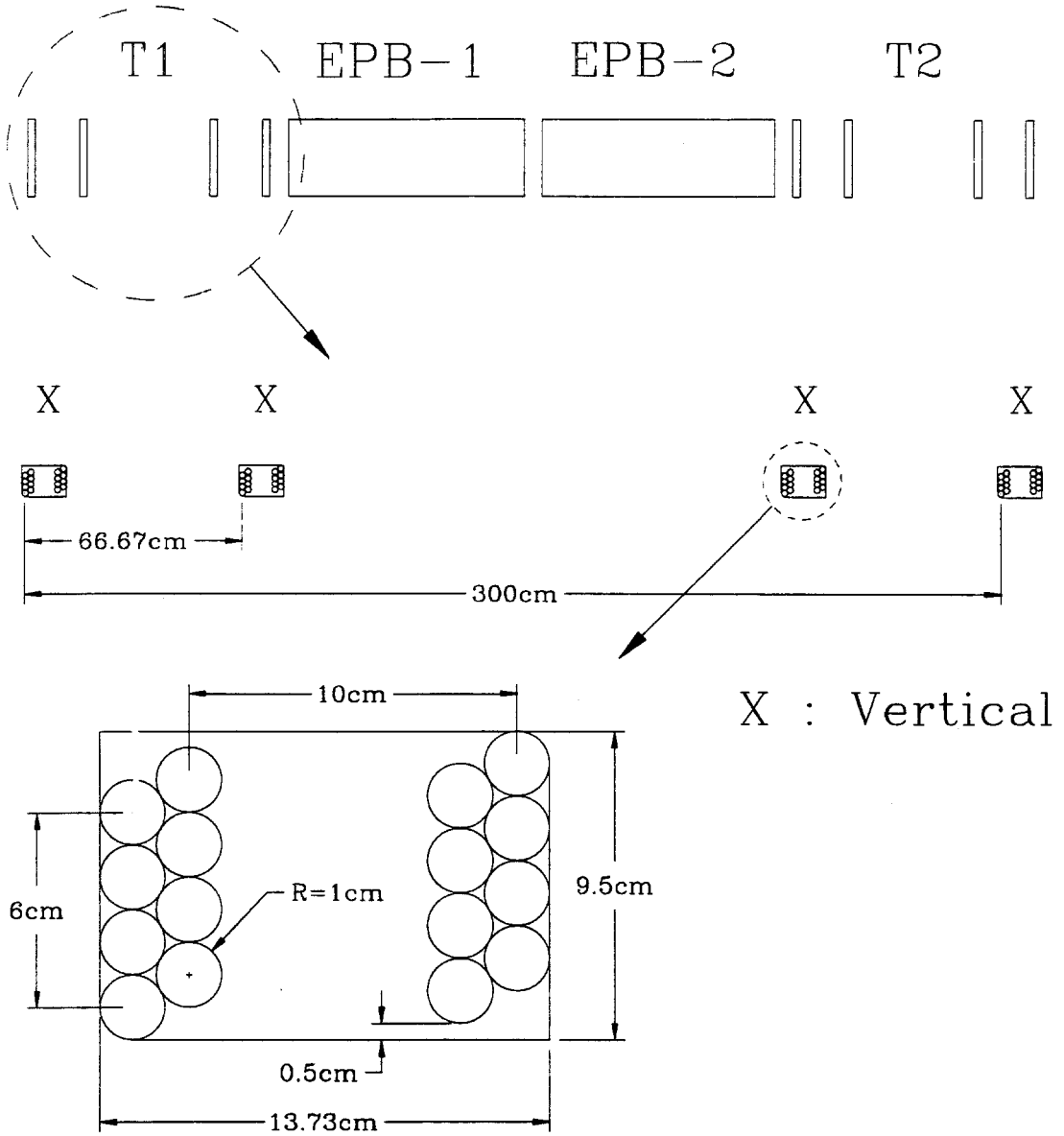

Figure 20: Schematic showing the straw tracking system for the upstream spectrometer.

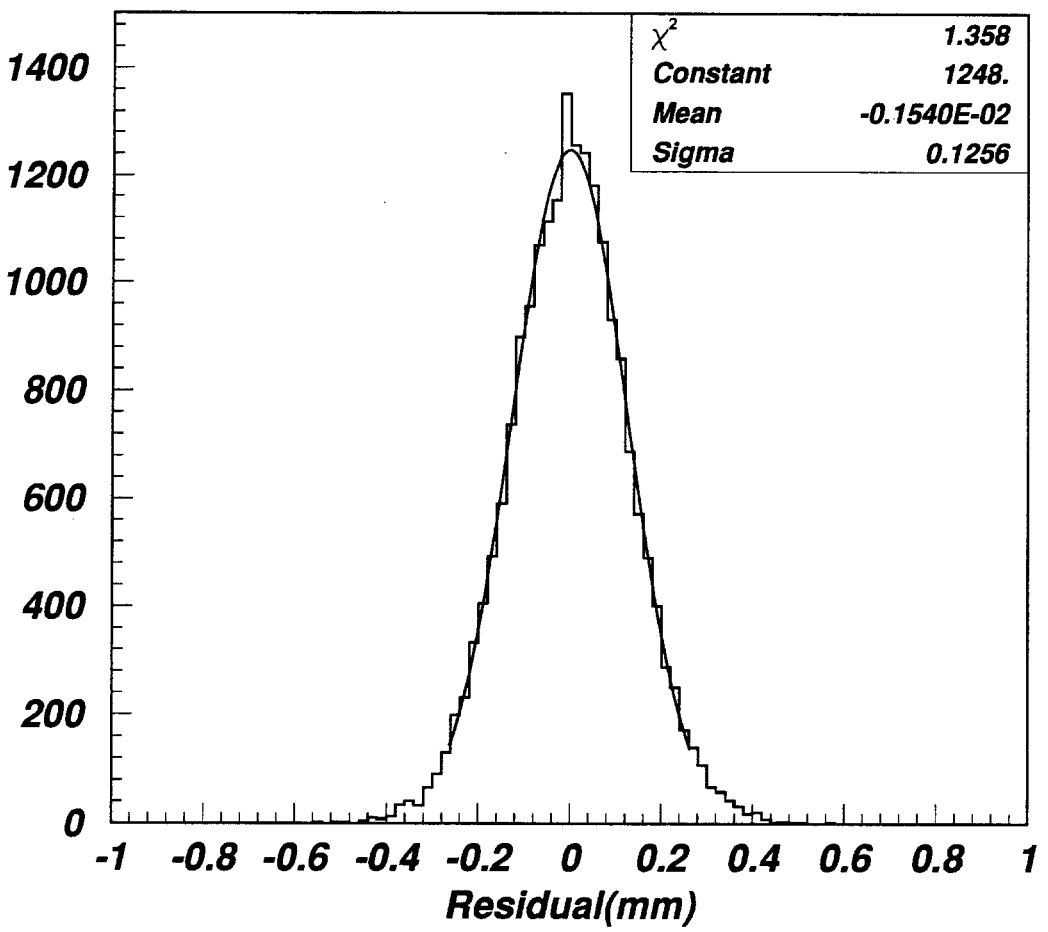

Figure 21: Spatial resolution of straw tubes (mm) measured for an SDC prototype tracking chamber.

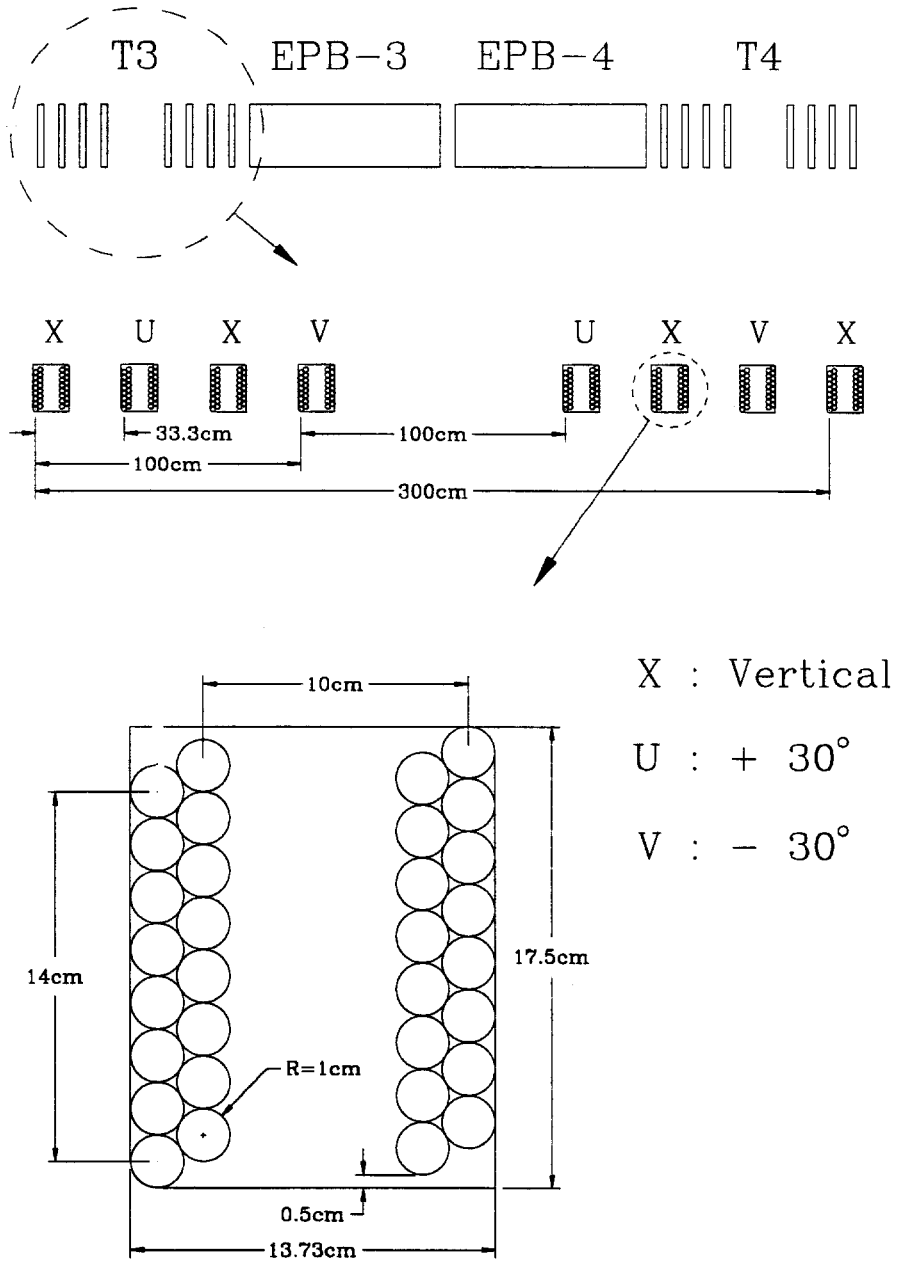

Figure 22: Schematic of the straw tracking system for the downstream spectrometer.

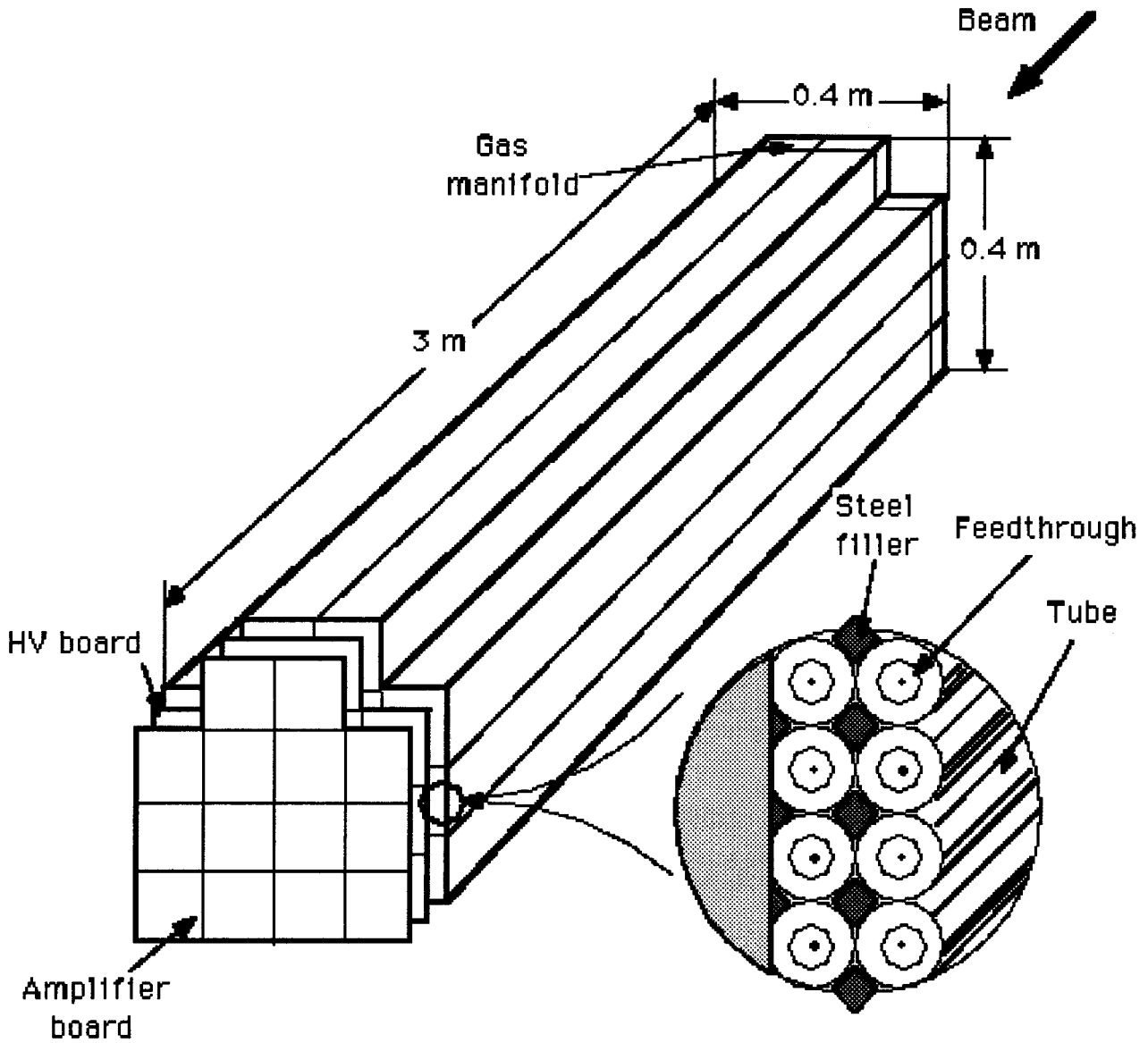

Figure 23: Schematic of the high pressure gas tube hadronic calorimeter showing the arrangement of the 14 calorimeter modules.

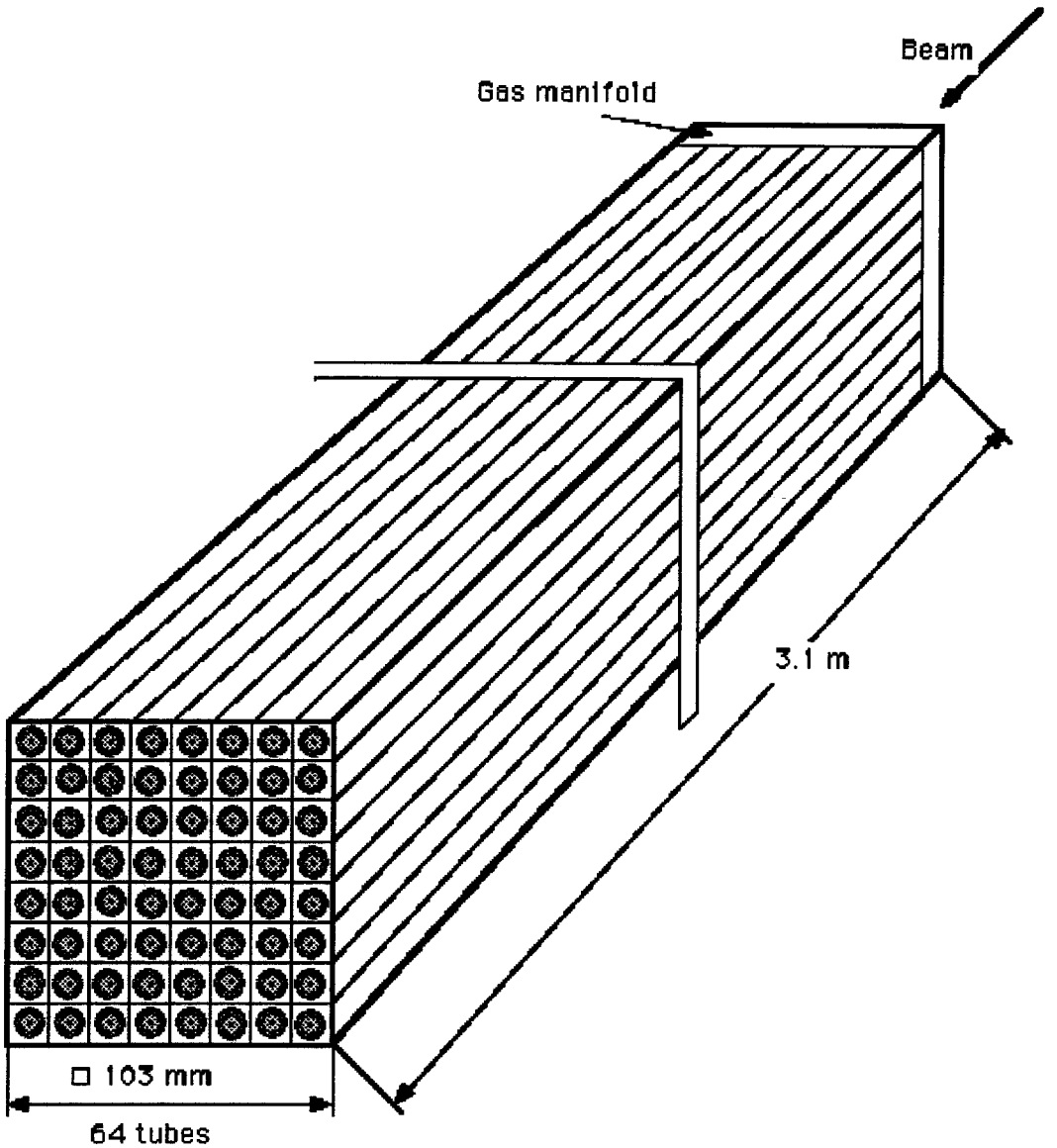

Figure 24: Schematic of a high pressure gas tube hadronic calorimeter module which is constructed from 64 tubes that are 3m long.

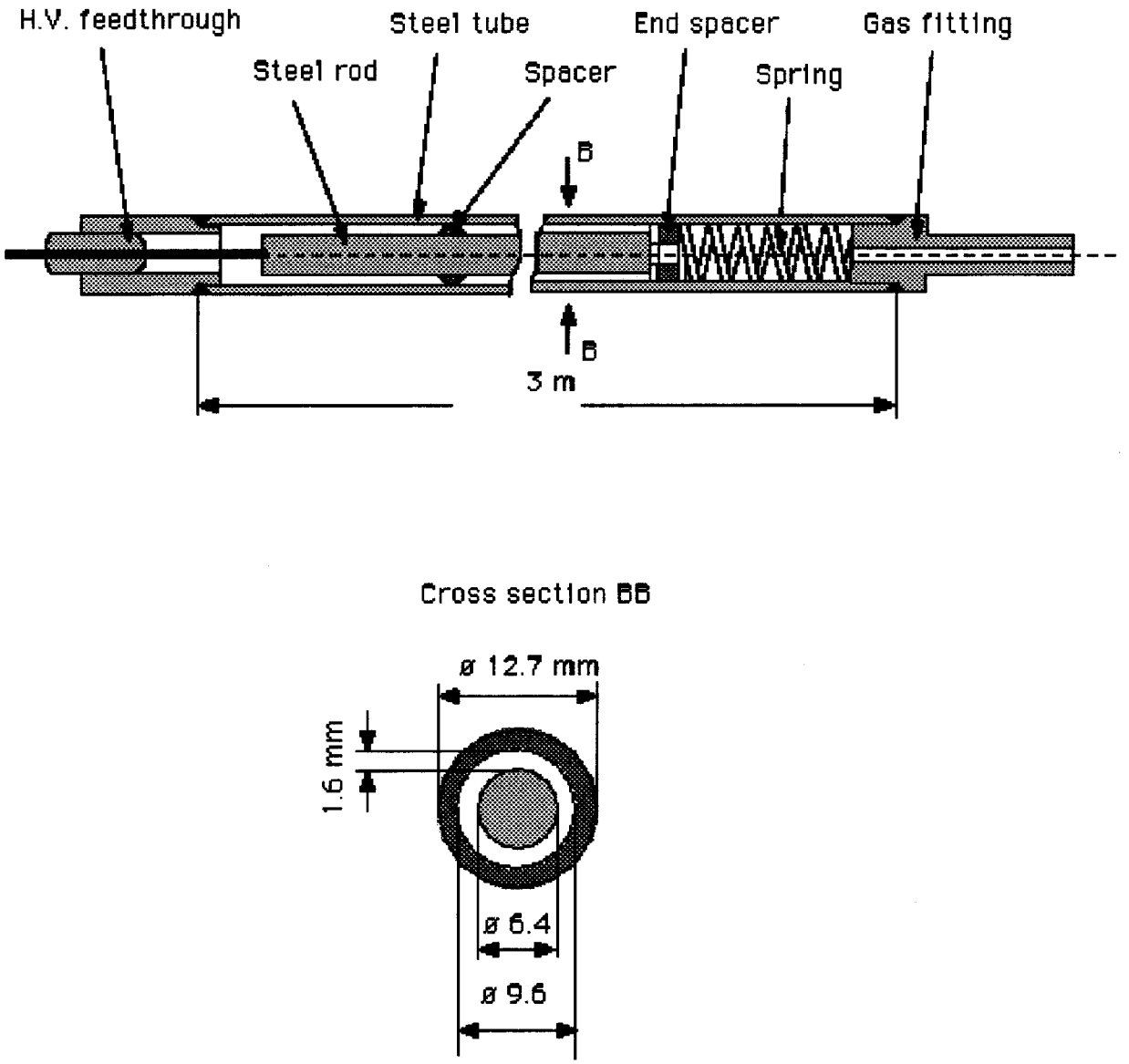

Figure 25: Schematic of a high pressure gas tube ionization chamber used in the hadronic calorimeter.

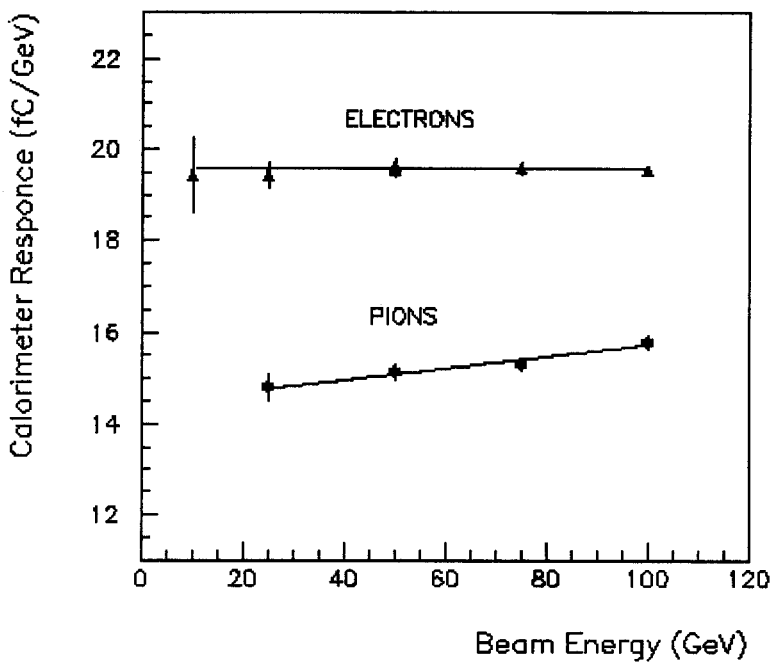

Figure 26: Testbeam results showing the linearity of the high pressure gas tube hadronic calorimeter.

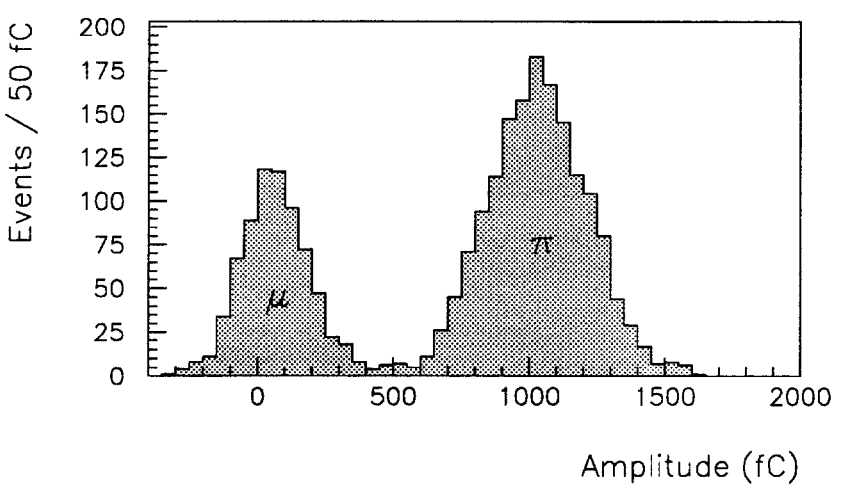

Figure 27: Testbeam results showing the response of the high pressure gas tube hadronic calorimeter to a 75 GeV beam containing pions and muons.

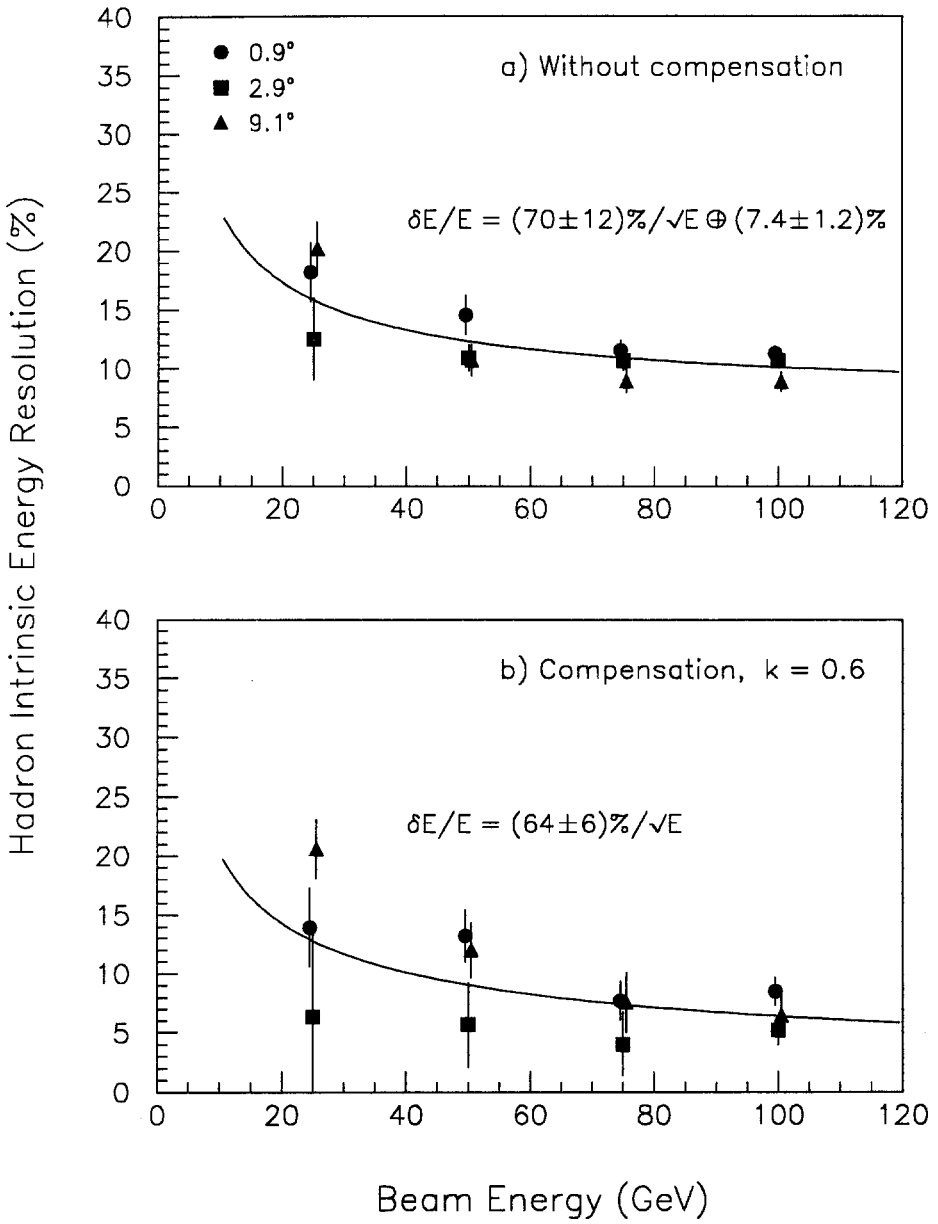

Figure 28: Testbeam results showing the intrinsic resolution of the high pressure gas tube hadronic calorimeter (a) before applying a software e/h compensation algorithm, and (b) after applying the algorithm.

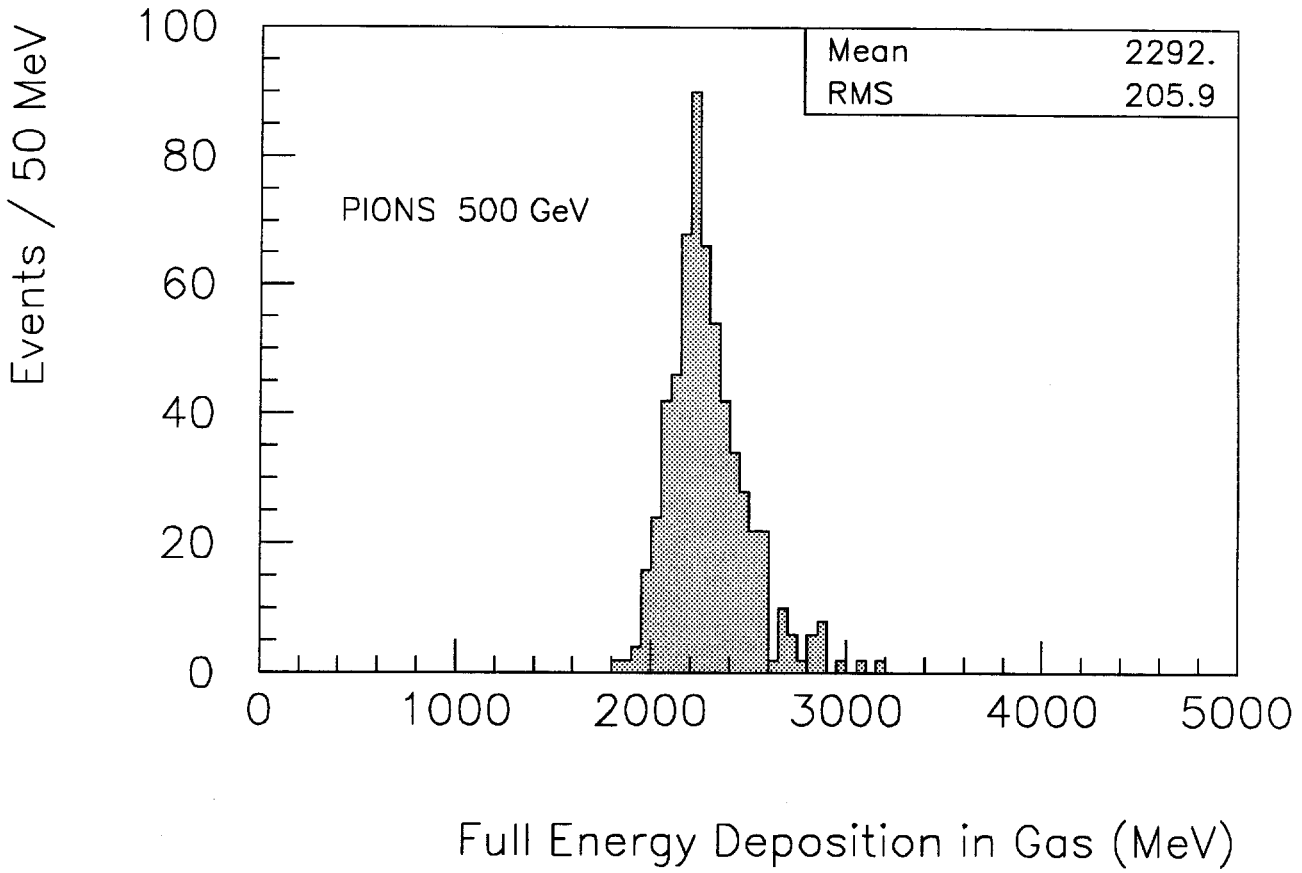

Figure 29: GEANT prediction for the response of the high pressure gas tube hadronic calorimeter to 500 GeV pions.

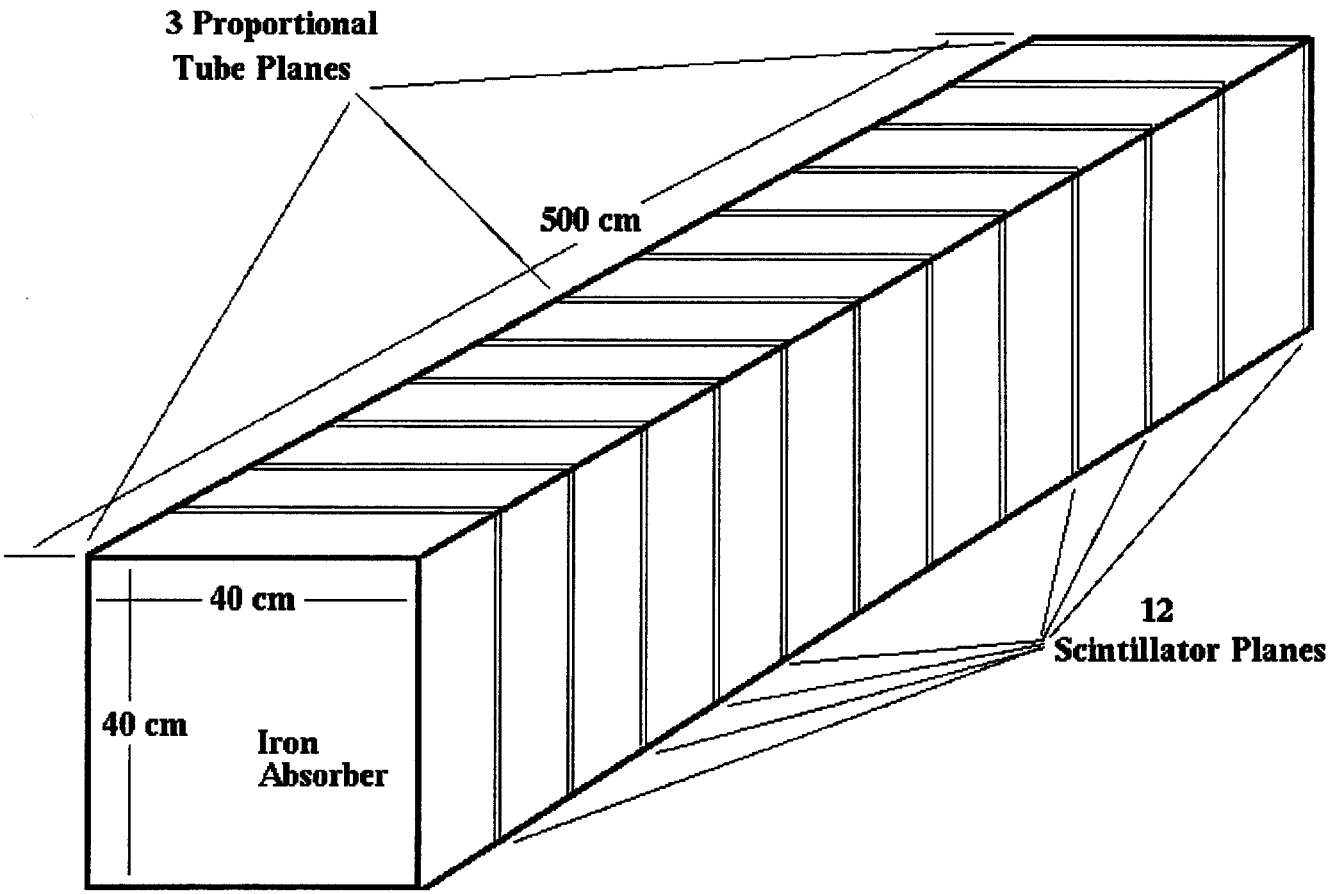

Figure 30: The Muon Tagger.

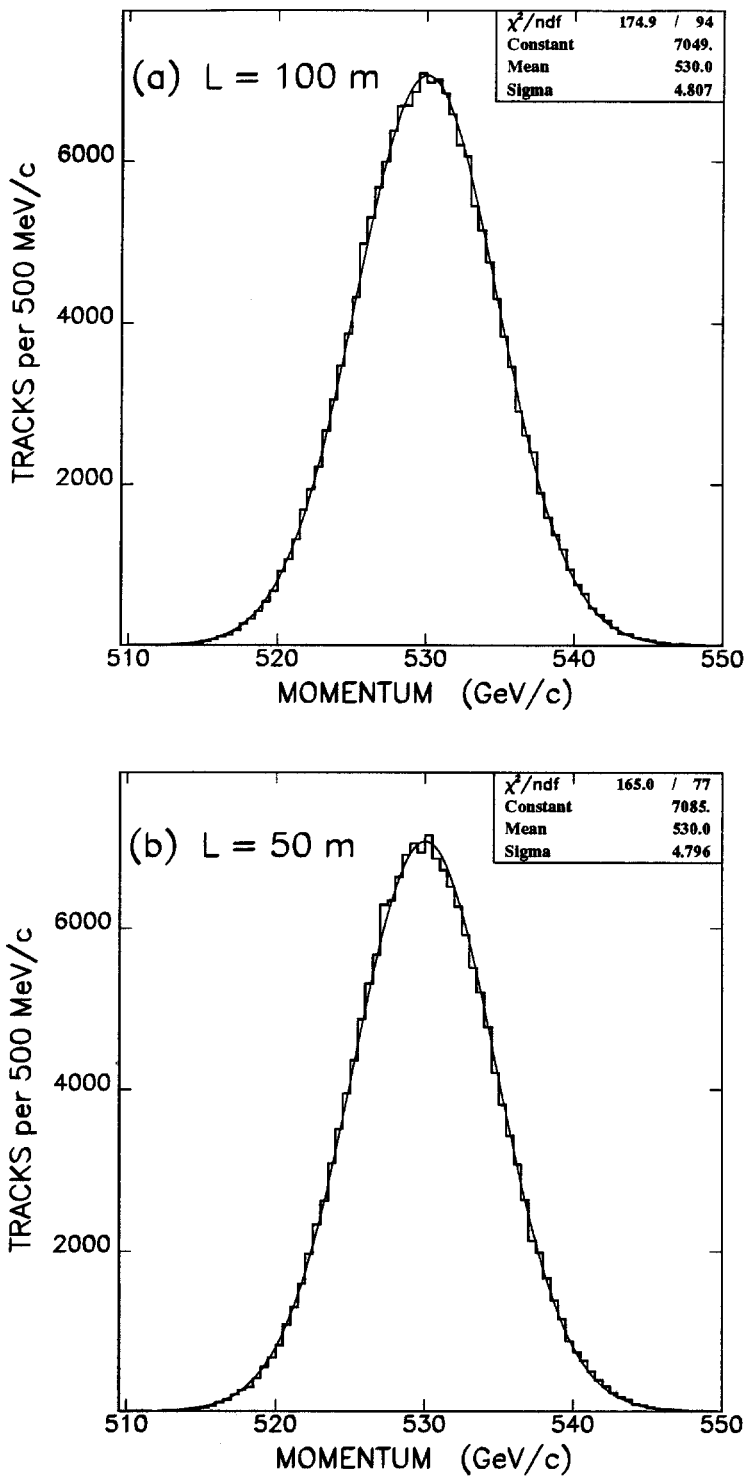

Figure 31: GEANT simulation of the distribution of momenta measured in the downstream momentum analyzer when 530 GeV/c pions are incident at the upstream end of the experiment (a) when the decay volume is 100m long, and (b) when the decay volume is 50m long.

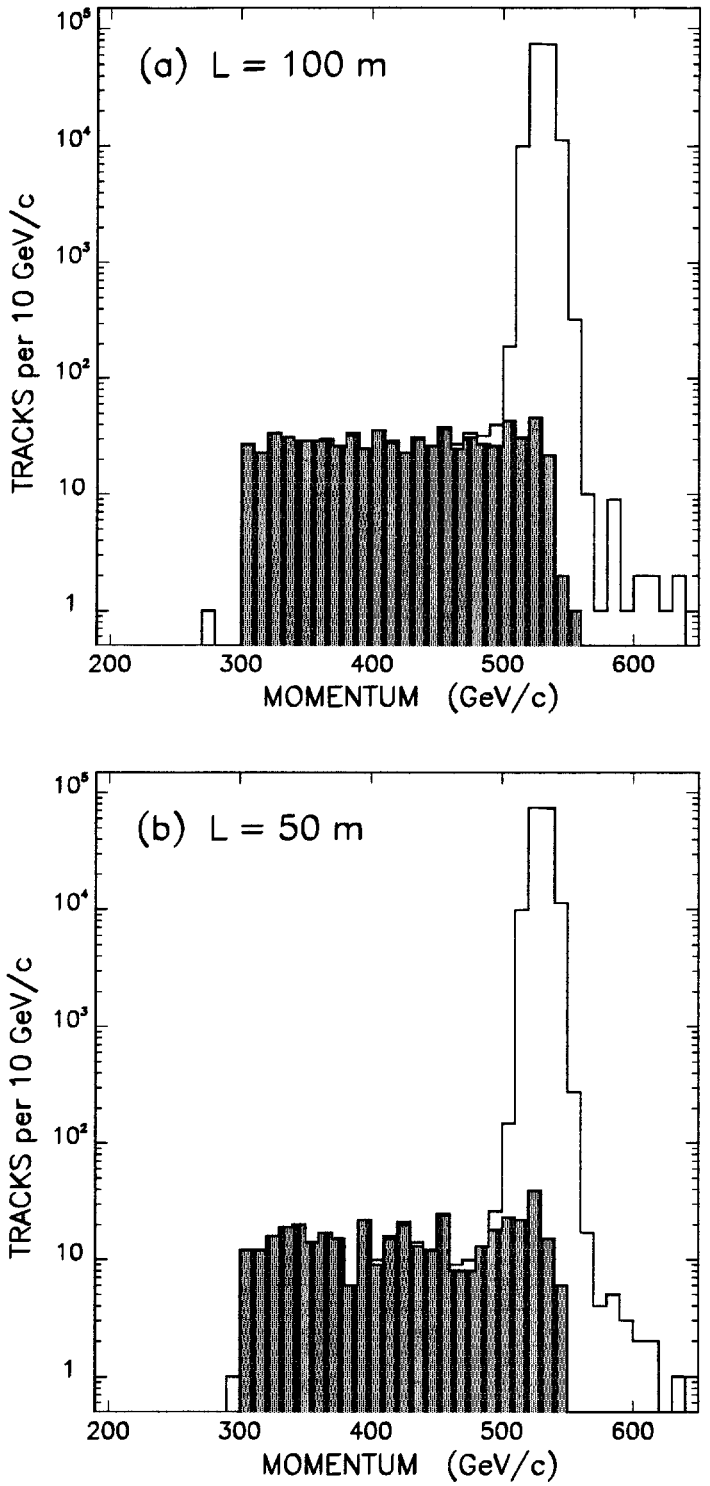

Figure 32: GEANT simulation of the distribution of momenta measured in the downstream momentum analyzer when 530 GeV/c pions are incident at the upstream end of the experiment (a) when the decay volume is 100m long, and (b) when the decay volume is 50m long. The shaded subhistograms show the contributions to the distributions from decay muons.

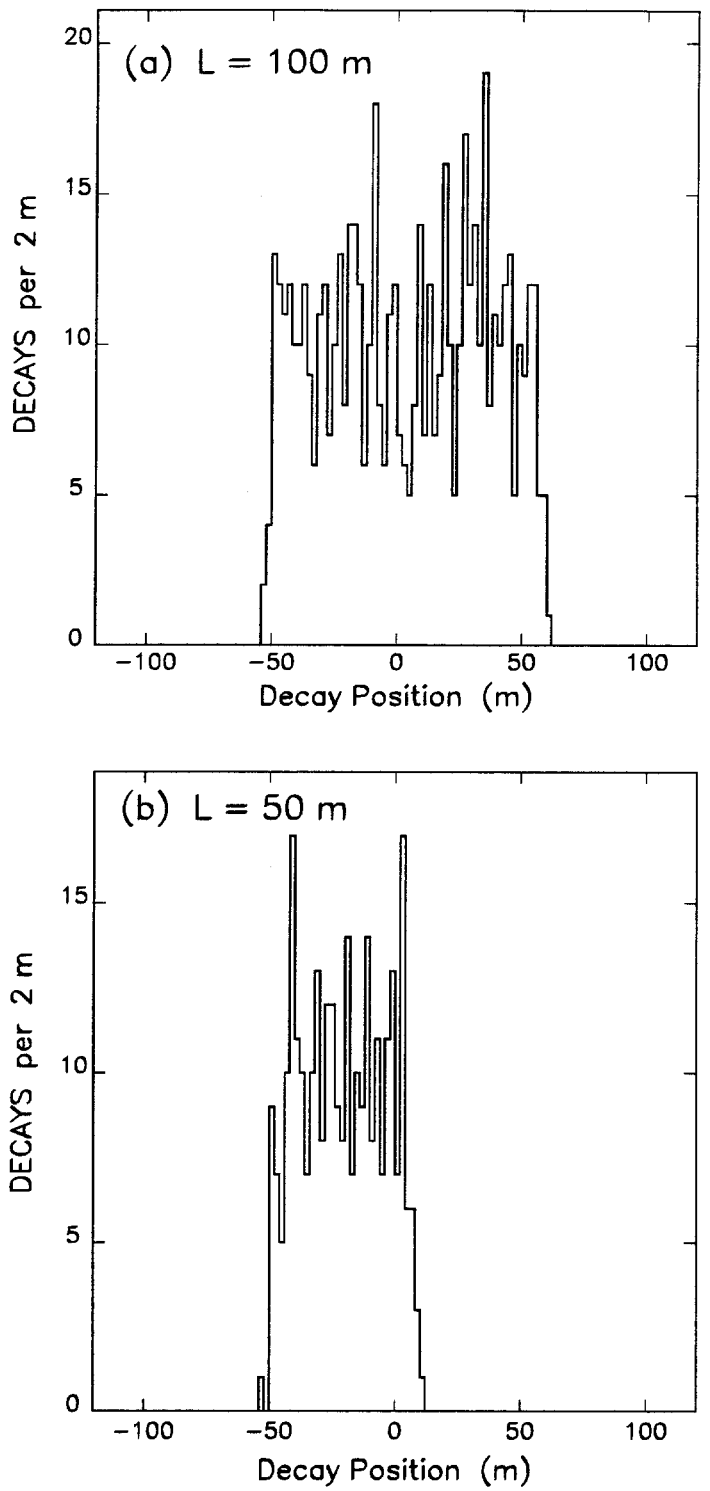

Figure 33: GEANT simulation of the spatial distribution of decay vertices for $\pi^{\pm} \rightarrow \mu\nu$ decay candidates measured by the proposed experiment when 530 GeV/c pions are incident on the upstream end of the apparatus and (a) the decay volume is 100m long, or (b) the decay volume is 50m long.